

Interaction Between an Optically Levitated Nanoparticle and Its Thermal Image: Internal Thermometry via Displacement Sensing

Thomas Agrenius, Carlos Gonzalez-Ballester, Patrick Maurer, and Oriol Romero-Isart

Institute for Quantum Optics and Quantum Information of the Austrian Academy of Sciences, A-6020 Innsbruck, Austria and

Institute for Theoretical Physics, University of Innsbruck, A-6020 Innsbruck, Austria

(Dated: September 26, 2022)

We propose and theoretically analyze an experiment where displacement sensing of an optically levitated nanoparticle in front of a surface can be used to measure the induced dipole-dipole interaction between the nanoparticle and its thermal image. This is achieved by using a surface that is transparent to the trapping light but reflective to infrared radiation, with a reflectivity that can be time modulated. This dipole-dipole interaction relies on the thermal radiation emitted by a silica nanoparticle having sufficient temporal coherence to correlate the reflected radiation with the thermal fluctuations of the dipole. The resulting force is orders of magnitude stronger than the thermal gradient force and it strongly depends on the internal temperature of the nanoparticle for a particle-to-surface distance greater than two micrometers. We argue that it is experimentally feasible to use displacement sensing of a levitated nanoparticle in front of a surface as an internal thermometer. Experimental access to the internal physics of a levitated nanoparticle in vacuum is crucial to understand the limitations that decoherence poses to current efforts devoted to prepare a nanoparticle in a macroscopic quantum superposition state.

Today, it is experimentally possible to optically levitate a nanoparticle in vacuum [1] and (i) feedback-cool its center-of-mass motion to the ground state [2–6], (ii) place it near a surface [7–13], (iii) measure the induced dipole-dipole interaction with another nanoparticle levitated in a second optical tweezer [14], and (iv) use displacement sensing to detect forces in the zeptonewton regime [15–21]. In this Letter, we propose to combine these experimental capabilities to measure the dipole-dipole interaction of an optically levitated nanoparticle with its *thermal* image (see Fig. 1a). This interaction depends on the internal temperature of the nanoparticle for particle-to-surface distances comparable to the thermal wavelength. Hence, we propose to leverage displacement sensing for internal thermometry of a levitated nanoparticle in vacuum [22–26].

Our proposal aims not only at experimentally measuring an out-of-equilibrium Casimir force, which has been the object of intense research [30–37], but also at giving experimental access to the internal physics of a levitated nanoparticle in vacuum which is very relevant for the field of levitodynamics [1, 38]. Knowledge of the internal temperature T of a nanoparticle and the imaginary part of its polarizability $\text{Im}\{\alpha\}$ in the infrared regime is essential to quantify one of the most limiting sources of decoherence for experiments aiming to prepare a macroscopic quantum superposition of a nanoparticle [28, 39–47]: decoherence due to thermal emission of photons [28, 40, 48, 49]. The associated decoherence rate approximately scales with T^6 and critically depends on $\text{Im}\{\alpha\}$. In addition, the calculation of non-equilibrium Casimir forces, decoherence due to thermal emission of photons, and internal temperature dynamics in vacuum all depend on the so-called local equilibrium assumption and the use of the fluctuation-dissipation theorem. That is, these calculations assume that the nanoparticle internally equilibrates faster than any other relevant

timescale and thus an internal temperature T can be defined. Whether this assumption holds for a nanoparticle in vacuum or not is a question that needs to be answered experimentally [50]. Our experimental proposal would test this assumption and its consequences.

More specifically, we propose to optically trap a silica glass nanoparticle of radius r and mass m at a distance z from a surface which is transparent at optical wavelengths but reflective at thermal (infrared) wavelengths, as illustrated in Fig. 1(a). We assume that the interaction between the nanoparticle and the electromagnetic field of wavelengths λ can be treated in the dipole approximation ($r \ll \lambda$) with isotropic polarizability $\alpha(\lambda)$, which we calculate from bulk electric permittivity data $\epsilon(\lambda)$ for silica glass [27] using $\alpha(\lambda) = 3V\epsilon_0[\epsilon(\lambda) - 1][\epsilon(\lambda) + 2]^{-1}$, where ϵ_0 is the vacuum permittivity and V the volume of the nanoparticle. We display $\text{Im}\{\alpha(\lambda)\}$ for infrared and optical wavelengths in Fig. 1(c). As we show later, the wavelength-dependent reflectivity of the surface gives rise to an image dipole interacting with the nanoparticle at the thermal wavelengths but not at the optical wavelengths. By using a surface with an infrared reflectivity that can be modulated in time, such as demonstrated in [51], we can furthermore modulate the interaction strength with the thermal dipole in time (Fig. 1(b)). The transparency of the surface at optical frequencies avoids an interaction force between the nanoparticle and its optical image, similar to the one observed in [14], the strength of which would dominate over the non-equilibrium Casimir forces we seek to measure [52]. Similarly, since the charge on optically levitated nanoparticles can be controlled [53], we propose to use electrically neutral particles to avoid interactions with the electrostatic mirror image [10]. We note that all-optical cold damping schemes for electrically uncharged silica nanoparticles have recently been demonstrated [5, 54].

In order to evaluate the force acting on the particle

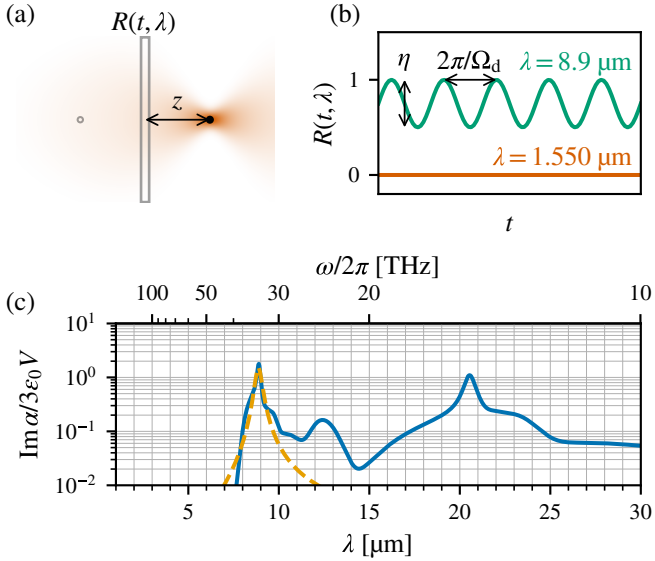


FIG. 1. (a) Illustration of the proposed experiment. A nanoparticle is optically trapped at a distance z from a surface with time- and wavelength-dependent reflection coefficient $R(t, \lambda)$. The effect of the surface can be approximated by the mirror image nanoparticle on the left. (b) The surface is transparent at the trapping wavelength, but is nearly perfectly reflecting at the peak wavelength of the nanoparticle's thermal emission. Additionally, the reflection coefficient of the surface at this wavelength can be modulated sinusoidally in time with frequency Ω_d and amplitude η . (c) The imaginary part of the polarizability of an SiO_2 nanoparticle in the optical and infrared region of the spectrum using the model of $\epsilon(\lambda)$ from [27] (solid line). For $\lambda \in [1, 7] \mu\text{m}$, the imaginary part of the polarizability is smaller than the lower limit of the graph [27]. At $\lambda = 1.550 \mu\text{m}$ we use $\text{Im}\{\alpha\}/(3\epsilon_0 V) = 1.5 \times 10^{-9}$ based on data reported in [28, 29]. The properties of the nanoparticle's infrared radiation is dominated by the peak at $8.9 \mu\text{m}$, to which we fit a Lorentzian function (dashed line).

in this scenario, we use the theory of fluctuational electrodynamics [31–35, 37, 55]. The steps we perform are summarized as follows (more details are given in [52]): We treat the nanoparticle as an electric dipole \mathbf{d} which has a part induced by the electric field \mathbf{d}_{ind} and a thermally fluctuating part \mathbf{d}_{th} . The total electric field \mathbf{E} is composed of a fluctuating field from the radiation of the nanoparticle \mathbf{E}_{ind} , a second fluctuating field from thermal radiation from the environment \mathbf{E}_{th} , and a non-fluctuating field due to the presence of the optical tweezer \mathbf{E}_{tw} . The force acting on the nanoparticle is the expectation value of the standard force on an electric dipole in an electric field: $\mathbf{F} = \sum_{j \in \{x, y, z\}} \langle d_j(t) \nabla E_j(\mathbf{r}_0, t) \rangle$, where \mathbf{r}_0 is the equilibrium position of the dipole. To evaluate this expression, we diagonalize the total dipole moment $\mathbf{d}(t)$ and field $\mathbf{E}(\mathbf{r}_0, t)$ in terms of the input quantities: \mathbf{d}_{th} and \mathbf{E}_{th} , whose correlations we assume to be given by the fluctuation-dissipation theorem, and \mathbf{E}_{tw} . This is possible by transforming to the

frequency domain where $\mathbf{d}_{\text{ind}}(\omega) = \alpha(\omega) \mathbf{E}(\mathbf{r}_0, \omega)$ and $\mathbf{E}_{\text{ind}}(\mathbf{r}, \omega) = \mathbf{G}(\mathbf{r}, \mathbf{r}_0, \omega) \mathbf{d}(\omega)$, with $\omega = 2\pi c/\lambda$, c the speed of light in vacuum, and $\alpha(\omega)$ defined in terms of $\alpha(\lambda = 2\pi c/\omega)$ (see top axis of Fig. 1(c)). Here $\mathbf{G}(\mathbf{r}, \mathbf{r}_0, \omega)$ is the electromagnetic Green's tensor. The presence of the surface modifies the Green's tensor, adding a scattering part \mathbf{G}_1 to the free-space Green's tensor \mathbf{G}_0 so that $\mathbf{G} = \mathbf{G}_0 + \mathbf{G}_1$. In accordance with our assumptions about the spectral reflectivity profile of the surface, we take $\mathbf{G}_1 \approx 0$ at optical frequencies, and \mathbf{G} to be the Green's tensor above a perfectly reflecting interface at thermal frequencies. After diagonalization, one finds $\mathbf{d}(\omega) = \mathbf{T}(\mathbf{r}_0, \omega) \{ \mathbf{d}_{\text{th}}(\omega) + \alpha(\omega) [\mathbf{E}_{\text{tw}}(\mathbf{r}_0, \omega) + \mathbf{E}_{\text{th}}(\mathbf{r}_0, \omega)] \}$, and $\mathbf{E}(\mathbf{r}, \omega) = \mathbf{E}_{\text{tw}}(\mathbf{r}, \omega) + \mathbf{E}_{\text{th}}(\mathbf{r}, \omega) + \mathbf{G}(\mathbf{r}, \mathbf{r}_0, \omega) \mathbf{d}(\omega)$. The tensor $\mathbf{T}(\mathbf{r}_0, \omega) \equiv [\mathbf{1} - \alpha(\omega) \mathbf{G}_1(\mathbf{r}_0, \mathbf{r}_0, \omega)]^{-1}$ accounts for multiple reflections between the surface and the dipole. \mathbf{F} can now be evaluated with the fluctuation-dissipation relations $\langle d_{j,\text{th}}(\omega) d_{k,\text{th}}(\omega') \rangle = 2\pi\hbar\delta(\omega - \omega') [2n(\omega, T) + 1] \text{Im}\{\alpha(\omega)\} \delta_{jk}$ and $\langle E_{j,\text{th}}(\mathbf{r}, \omega) E_{k,\text{th}}(\mathbf{r}_0, \omega') \rangle = 2\pi\hbar\delta(\omega - \omega') [2n(\omega, T_{\text{env}}) + 1] \text{Im}\{G_{jk}(\mathbf{r}, \mathbf{r}_0, \omega)\}$. Here $n(\omega, T)$ is the Bose-Einstein distribution, \hbar is the reduced Planck's constant, and T and T_{env} are the temperatures of the nanoparticle and the electromagnetic environment respectively. The quantities \mathbf{E}_{th} , \mathbf{d}_{th} , and \mathbf{E}_{tw} are assumed to have vanishing cross-correlations.

With this method, the total force \mathbf{F} on the nanoparticle is found to have five contributions (see [52] for details): (1) the optical force from the optical tweezer, (2) an interaction force between the nanoparticle and its optical mirror image, which is negligible in our scenario due to the assumption $\mathbf{G}_1 \approx 0$ at optical frequencies (an assumption we further discuss and justify in [52]), (3) the zero-temperature Casimir force between the surface and the nanoparticle, (4) a force due to interaction with environmental thermal radiation which depends on T_{env} , and (5) a force due to interaction between the nanoparticle and its reflected thermal radiation, or equivalently, its thermal mirror image. The last contribution depends on the nanoparticle internal temperature T , and we will denote it as $\mathbf{F}_{\text{rad}}(T, z)$. Since the subwavelength nanoparticle scatters radiation only weakly, reflections beyond the first order turn out to have a negligible impact on the forces and one can approximate $\mathbf{T}(\mathbf{r}_0, \omega) \approx \mathbf{1}$ (see [52]). In this approximation, \mathbf{F}_{rad} is given by [52]

$$\mathbf{F}_{\text{rad}}(T, z) = \frac{\mathbf{e}_z \hbar c}{4\pi\epsilon_0 z^4} \int_0^\infty \frac{d\lambda}{\lambda^2} \frac{\text{Im}\{\alpha(\lambda)\} f(2\pi z/\lambda)}{\exp[2\pi\hbar c/(k_B T \lambda)] - 1}, \quad (1)$$

where \mathbf{e}_z is the surface normal vector, k_B is Boltzmann's constant, and $f(x)$ is the oscillatory dimensionless function $f(x) = \text{Re} \{ \exp(2ix) (-3 + 6ix + 6x^2 - 4ix) \}$. The expressions of the other four contributions to \mathbf{F} are given in [52].

In Fig. 2, we plot $\mathbf{e}_z \cdot \mathbf{F}$ as a function of z and T in the range 300 to 1500 K with increments of 100 K. We assume $T_{\text{env}} = 300$ K. Note that therefore the black line ($T = 300$ K) corresponds to the equilibrium case. We find that as T is increased, the total force becomes dom-

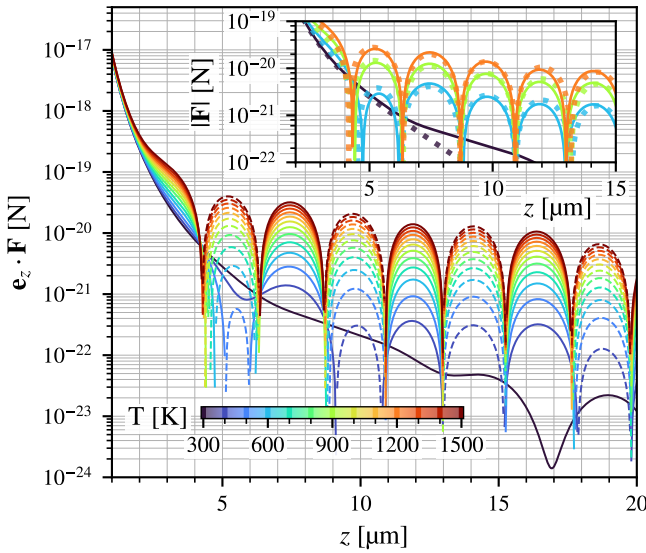


FIG. 2. The total dipole force on the nanoparticle along the direction normal to the surface when $R(t, \lambda) = 1$ for $\lambda \geq 7 \mu\text{m}$, using the full spectral dependence of $\alpha(\omega)$ (solid line in Fig. 1(c)). Solid/dashed lines indicate that the force is repulsive/attractive. The $T = 300 \text{ K}$ curve (black) is the force on the particle in equilibrium since we assume that $T_{\text{env}} = 300 \text{ K}$. Inset: Comparison of the total dipole force on the nanoparticle computed using the full spectral dependence (lines) versus the Lorentzian fit (dots) of $\alpha(\omega)$ as shown in Fig. 1(b).

inated by the T -dependent fifth contribution \mathbf{F}_{rad} . Only at the smallest distances $z \lesssim 2 \mu\text{m}$ is the temperature dependence lost. This is due to the dominance of the zero-temperature Casimir force component over all the other force contributions at small separations [35, 36, 55]. At distances $z > 2 \mu\text{m}$, the force scales more slowly with distance than the z^{-5} scaling characteristic of zero-temperature Casimir–Polder forces [35, 56]. Additionally, we observe that the force oscillates in sign along z with a temperature-independent period. The oscillations arise due to the peak at $\lambda_{\text{peak}} = 8.9 \mu\text{m}$ of $\text{Im}\{\alpha(\lambda)\}$ (which is attributed to vibrations of the Si–O bond in silica glass [27]) dominating the integral in Eq. (1) for $T \gtrsim 400 \text{ K}$. To confirm this explanation, we fit a Lorentzian function centered at λ_{peak} to $\text{Im}\{\alpha(\lambda)\}$, finding that the fit has full width at half maximum (FWHM) of $0.4 \mu\text{m}$ (dashed curve in Fig. 1(c)). We then compare the total force calculated with this fitted Lorentzian function and the force using $\alpha(\lambda)$ in the inset of Fig. 2, finding excellent agreement when the temperature of the nanoparticle is above 400 K . We remark that the oscillatory nature of the force could be utilized to perform a measurement of the distance from the nanoparticle to the surface.

We emphasize that the interaction giving rise to \mathbf{F}_{rad} is of temporally coherent nature [14]. That is, the thermal dipole moment $\mathbf{d}_{\text{th}}(t)$ remains correlated with itself dur-

ing the time it takes for the thermally emitted radiation to be reflected by the surface and return to the particle: in time domain, $\mathbf{E}_{\text{ind}}(t) = \int_{-\infty}^{\infty} dt' \mathbf{G}(t - t') \mathbf{d}(t')$, and therefore $\mathbf{F}_{\text{rad}} \propto \langle d_{\text{th},j}(t) d_{\text{th},k}(t') \rangle$. The temporal coherence of the nanoparticle’s thermal radiation is endowed by the narrow frequency spectrum of $\text{Im}\{\alpha\}$. A hypothetical increasingly broadband emitter, with accordingly shorter coherence time, would produce a force \mathbf{F}_{rad} with weakening oscillations which in the white-noise limit $\langle d_{\text{th},j}(t) d_{\text{th},k}(t') \rangle \rightarrow \delta(t - t')$, tends to zero since the time-domain Green’s tensor vanishes for zero time argument. Additionally, we point out that \mathbf{F}_{rad} cannot be written as the gradient of an electromagnetic field intensity [57, 58]. The gradient force that the nanoparticle experiences due to its radiated field intensity is a higher-order term in the tensor $\mathbf{T}(\mathbf{r}_0, \omega)$ which is not included in Eq. (1) and the contribution of which to \mathbf{F} is negligible.

Fig. 2 shows that \mathbf{F} reaches values above 10^{-21} N , the currently demonstrated sensitivity in dynamic force sensing experiments with optically levitated nanoparticles in vacuum [2–4, 15–17, 19, 21, 59, 60], for a wide range of temperatures T and particle-surface separations z . This suggests that $\mathbf{F}_{\text{rad}}(T, z)$ can be measured with current laboratory capabilities. The thermally limited force sensitivity \mathcal{S} is defined as the magnitude of an external oscillating force which if applied to the nanoparticle would give a contribution to the nanoparticle’s motional power spectral density (PSD) of the same magnitude as the thermally driven motional PSD, that is $\mathcal{S} = \sqrt{S_{\text{noise}}}$, where S_{noise} is the PSD of the thermal forces acting on the nanoparticle. Under cold damping of the nanoparticle motion, the leading thermal forces are impacts with residual gas molecules and photon shot noise [60], and it can be shown that [52]

$$\mathcal{S} = \sqrt{\frac{2\hbar P_{\text{scatt}}}{5c\lambda_0} + \frac{m\gamma_{\text{gas}}k_{\text{B}}T_{\text{env}}}{\pi}}. \quad (2)$$

Here P_{scatt} is the power that the nanoparticle scatters from the laser beam of wavelength λ_0 [60], and γ_{gas} is the damping rate due to collisions with gas molecules, directly proportional to the vacuum chamber pressure p [61]. We assume that the contributions from other sources of noise (e.g. surface-induced noise on neutral particles [62]) are negligible compared to the photon shot

TABLE I. Table of proposed experimental parameters.

Parameter	Value
nanoparticle radius r	100 nm
nanoparticle density ρ	2200 kg m ⁻³
environment temperature T_{env}	300 K
gas pressure p_*	10^{-10} mbars
tweezer wavelength λ_0	1.550 μm
numerical aperture N	0.75
laser power P_{tw}	10 mW
reflection modulation amplitude η	0.5
driving frequency Ω_d	$2\pi \times 12 \text{ kHz}$
driving quality factor Q	10^6

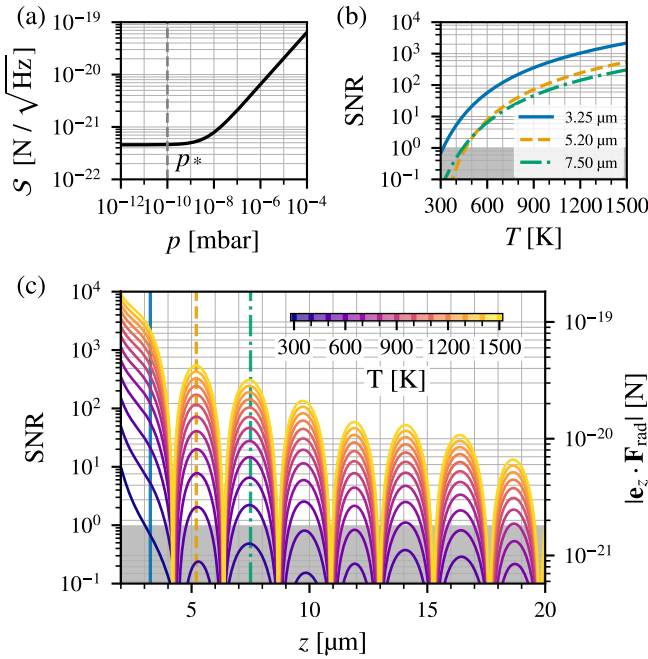


FIG. 3. (a) The force sensitivity as a function of the ambient gas pressure. The vertical dashed line identifies p_* , the pressure below which the sensitivity is photon shot-noise limited. We use p_* for plotting the other panels. (b) The signal-to-noise ratio (SNR) as a function of the nanoparticle internal temperature for three selected values of z . The gray area indicates the limit of measurability ($\text{SNR} < 1$). (c) The force (right y-axis) and SNR (left y-axis) as a function of z for $T = 300 \text{ K}, 400 \text{ K}, \dots, 1500 \text{ K}$. The grid lines follow the force axis. The vertical lines indicate the selected values of z for which the full T -dependence is displayed in panel (b).

noise. In Fig. 3(a) we show that for the choice of experimental parameters presented in Table I, zeptonewton force sensitivity is achieved for $p \leq 10^{-9}$ mbar with saturation to the photon shot noise limit $4 \times 10^{-22} \text{ N}/\sqrt{\text{Hz}}$ at $p_* = 10^{-10}$ mbar. We assume this value of the pressure for the remainder of the discussion.

In order to generate a time-oscillating force that can be dynamically measured, we propose to modulate the reflection coefficient $R(t, \lambda) = 1 - \eta[1 - \cos(\Omega_d t)]/2$ [63] of the surface at relevant infrared wavelengths. As we show in [52], by assuming that $\partial_\lambda R(t, \lambda) = 0$ across the $0.4 \mu\text{m}$ FWHM of the $8.9 \mu\text{m}$ peak of $\text{Im}\{\alpha(\lambda)\}$, \mathbf{F}_{rad} splits into an average force and a time-dependent force $\eta|\mathbf{F}_{\text{rad}}(T, z)| \cos(\Omega_d t)/2$. The result is the appearance of a peak in the motional PSD at the frequency Ω_d whose maximum is proportional to $|\mathbf{F}_{\text{rad}}|$. The ratio of this maximum to the thermally driven motional PSD defines the signal-to-noise ratio (SNR), which for $p \leq p_*$ becomes [52]

$$\text{SNR}(\Omega_d) = \frac{15cc_0^2}{256\pi^4\hbar} \frac{\lambda_0^7 Q \eta^2 |\mathbf{F}_{\text{rad}}(T, z)|^2}{\Omega_d |\alpha(\lambda_0)|^2 N^2 P_{\text{tw}}} \quad (3)$$

Here Q is the quality factor of the reflection coefficient modulation and P_{tw} is the optical tweezer power. We plot

the SNR as a function of T in Fig. 3(b) and as a function of z in Fig. 3(c). Fig. 3(b) shows that the force is measurable ($\text{SNR} > 1$) in the entire temperature range 300–1500 K for $z = 3.25 \mu\text{m}$, and at least in the range 400–1500 K for $z = 7.50 \mu\text{m}$. In Fig. 3(c), we observe that with the chosen parameters, the force remains measurable for temperatures above 800 K even at separations of $19 \mu\text{m}$ and above. Additionally, we see in Fig. 3(b) that the SNR depends strongly on the internal temperature T , changing by several orders of magnitude (depending on z) as the temperature is increased by a factor of 5.

These results show that measurement of the driven \mathbf{F}_{rad} provides a way to perform thermometry of the nanoparticle internal temperature in ultrahigh vacuum [22–26]. Due to absence of internal cooling by residual gas at p_* , the main heat dissipation channel of the nanoparticle will be radiative cooling. This opens up the prospect of investigating the radiative thermalization of the nanoparticle, similar to what was done for a silica nanofiber in [64], but here for an isolated (i.e. unclamped) nano-sized object. Questions about the nature of radiative thermalization of isolated nanoparticles have recently been raised [50], especially about the validity of the local equilibrium assumption. We theoretically study the radiative thermalization predicted by fluctuational electrodynamics (which includes the local equilibrium assumption) by writing down the heat balance equation $C\dot{T} = P_{\text{abs}} - P_{\text{rad}}(T)$, where $C = c_m \rho V$, is the heat capacity of the nanoparticle with $c_m = 700 \text{ J/kg}$ and ρ the specific heat capacity and density of silica glass, P_{abs} the power that the nanoparticle absorbs, and $P_{\text{rad}}(T)$ the power that the nanoparticle radiates. As shown in [52], $P_{\text{rad}}(T)$ calculated with $\text{Im}\{\alpha(\lambda)\}$ as displayed in Fig. 1(c) is approximately quadratic in the temperature range 300–2000 K: $P_{\text{rad}}(T) \approx \sigma_2 V T^2$ with the parameter $\sigma_2 = 2 \times 10^4 \text{ W/m}^3 \text{ K}^2$. Solving the heat balance equation with this approximation gives the qualitative time evolution of the particle's internal temperature

$$T(t) = \begin{cases} T_\infty \tanh[t/\tau + \text{artanh}(T_0/T_\infty)] & (T_\infty > T_0) \\ T_\infty \coth[t/\tau + \text{artanh}(T_\infty/T_0)] & (T_\infty < T_0) \end{cases} \quad (4)$$

where T_0 is the initial internal temperature, $T_\infty = \sqrt{P_{\text{abs}} \sigma_2 / V}$ is the steady-state temperature, and the time constant is $\tau = \rho c_m \sqrt{\sigma_2 V / P_{\text{abs}}}$, which we remark is independent of the nanoparticle size since $P_{\text{abs}} \propto \text{Im}\{\alpha(\lambda_0)\} \propto V$. With the parameters as in Table I, we find $T_\infty \approx 500 \text{ K}$ and $\tau \approx 0.2 \text{ s}$. Compared to numerical solution of the heat balance equation using the full $P_{\text{rad}}(T)$, the approximate solution gives qualitatively correct behavior of thermalization dynamics and correct steady-state temperatures within a margin of a few tenths of K [52]. In experiments, the internal temperature of the nanoparticle can be controlled independently from the optical trap power by using a dedicated heating laser [25]. Thus, the radiative cooling could be investigated by heating the particle to temperatures above the equilibrium temperature in the optical tweezer and then

monitoring the decay of the temperature via the decay of the SNR peak. Observing a departure from the radiative cooling described by Eq. (4) would be an indication of non-applicability of the local equilibrium assumption [50].

To conclude, we have proposed an experiment to measure an out-of-equilibrium Casimir force using an optically levitated nanoparticle in vacuum. We believe this is interesting *per se* given the challenge to measure these forces [36, 37, 65]. In addition, we have discussed how dynamic sensing of this force can be used to measure the internal temperature of the nanoparticle, both in the steady state as well as in a dynamical setting with radiative cooling taking place. Despite operating in the classical regime, we view the proposed experiment as highly relevant for current efforts to prepare large quantum superposition states of a levitated nanoparticle [28, 39–47]. The design of these protocols is constrained by decoherence due to thermal radiation. One can show that this decoherence rate is proportional to $\int_0^\infty d\lambda \lambda^{-7} n(T, \lambda) \text{Im}\{\alpha(\lambda)\}$ [49, 66], and hence critically

depends on both the nanoparticle internal temperature and polarizability at infrared frequencies. Our proposed experiment gives information on both properties; the latter since the decoherence rate shows a similar dependence on $\alpha(\lambda)$ as Eq. (1). In addition, the observation that the thermal radiation of the nanoparticle is dominated by a narrow wavelength range would enable new strategies for the management of center-of-mass decoherence. We are currently investigating the effect on the decoherence rate of suppressing the radiation at the peak thermal wavelength. We hope this work will trigger the realization of classical experiments with levitated nanoparticles that provide key information about the physics related to sources of decoherence, which we consider pivotal in enabling the ambitious goal of preparing a nanoparticle in a large quantum superposition state.

We thank Romain Quidant for suggesting to us the idea of modulating the surface reflection coefficient. This research has been supported by the European Research Council (ERC) under the grant Agreement No. [951234] (Q-Xtreme ERC-2020-SyG).

[1] C. Gonzalez-Ballester, M. Aspelmeyer, L. Novotny, R. Quidant, and O. Romero-Isart, Levitodynamics: Levitation and control of microscopic objects in vacuum, *Science* **374**, eabg3027 (2021).

[2] U. Delić, M. Reisenbauer, K. Dare, D. Grass, V. Vuletić, N. Kiesel, and M. Aspelmeyer, Cooling of a levitated nanoparticle to the motional quantum ground state, *Science* **367**, 892 (2020).

[3] L. Magrini, P. Rosenzweig, C. Bach, A. Deutschmann-Olek, S. G. Hofer, S. Hong, N. Kiesel, A. Kugi, and M. Aspelmeyer, Real-time optimal quantum control of mechanical motion at room temperature, *Nature* **595**, 373 (2021).

[4] F. Tebbenjohanns, M. L. Mattana, M. Rossi, M. Frimmer, and L. Novotny, Quantum control of a nanoparticle optically levitated in cryogenic free space, *Nature* **595**, 378 (2021).

[5] M. Kamba, R. Shimizu, and K. Aikawa, Optical cold damping of neutral nanoparticles near the ground state in an optical lattice, *Opt. Express* **30**, 26716 (2022).

[6] A. Ranfagni, K. Børkje, F. Marino, and F. Marin, Two-dimensional quantum motion of a levitated nanosphere, *Phys. Rev. Research* **4**, 033051 (2022).

[7] I. Alda, J. Berthelot, R. A. Rica, and R. Quidant, Trapping and manipulation of individual nanoparticles in a planar Paul trap, *Appl. Phys. Lett.* **109**, 163105 (2016).

[8] S. Kuhn, G. Wachter, F.-F. Wieser, J. Millen, M. Schneider, J. Schalko, U. Schmid, M. Trupke, and M. Arndt, Nanoparticle detection in an open-access silicon microcavity, *Appl. Phys. Lett.* **111**, 253107 (2017).

[9] R. Diehl, E. Hebestreit, R. Reimann, F. Tebbenjohanns, M. Frimmer, and L. Novotny, Optical levitation and feedback cooling of a nanoparticle at subwavelength distances from a membrane, *Phys. Rev. A* **98**, 013851 (2018).

[10] G. Winstone, R. Bennett, M. Rademacher, M. Rashid, S. Buhmann, and H. Ulbricht, Direct measurement of the electrostatic image force of a levitated charged nanoparticle close to a surface, *Phys. Rev. A* **98**, 053831 (2018).

[11] L. Magrini, R. A. Norte, R. Riedinger, I. Marinković, D. Grass, U. Delić, S. Gröblacher, S. Hong, and M. Aspelmeyer, Near-field coupling of a levitated nanoparticle to a photonic crystal cavity, *Optica* **5**, 1597 (2018).

[12] K. Shen, Y. Duan, P. Ju, Z. Xu, X. Chen, L. Zhang, J. Ahn, X. Ni, and T. Li, On-chip optical levitation with a metalens in vacuum, *Optica* **8**, 1359 (2021).

[13] C. Montoya, E. Alejandro, W. Eom, D. Grass, N. Clarisso, A. Witherspoon, and A. A. Geraci, Scanning force sensing at micrometer distances from a conductive surface with nanospheres in an optical lattice, *Appl. Opt.* **61**, 3486 (2022).

[14] J. Rieser, M. A. Ciampini, H. Rudolph, N. Kiesel, K. Hornberger, B. A. Stickler, M. Aspelmeyer, and U. Delić, Tunable light-induced dipole-dipole interaction between optically levitated nanoparticles, *Science* **377**, 987 (2022).

[15] T. Li, S. Kheifets, and M. G. Raizen, Millikelvin cooling of an optically trapped microsphere in vacuum, *Nature Phys.* **7**, 527 (2011).

[16] J. Gieseler, B. Deutsch, R. Quidant, and L. Novotny, Subkelvin parametric feedback cooling of a laser-trapped nanoparticle, *Phys. Rev. Lett.* **109**, 103603 (2012).

[17] J. Gieseler, L. Novotny, and R. Quidant, Thermal nonlinearities in a nanomechanical oscillator, *Nature Phys.* **9**, 806 (2013).

[18] D. C. Moore, A. D. Rider, and G. Gratta, Search for millicharged particles using optically levitated microspheres, *Phys. Rev. Lett.* **113**, 251801 (2014).

[19] G. Ranjit, M. Cunningham, K. Casey, and A. A. Geraci, Zeptoneutron force sensing with nanospheres in an optical lattice, *Phys. Rev. A* **93**, 053801 (2016).

[20] A. D. Rider, D. C. Moore, C. P. Blakemore, M. Louis, M. Lu, and G. Gratta, Search for screened interactions associated with dark energy below the 100 μm length scale, *Phys. Rev. Lett.* **117**, 101101 (2016).

[21] D. Hempston, J. Vovroš, M. Toroš, G. Winstone, M. Rashid, and H. Ulbricht, Force sensing with an optically levitated charged nanoparticle, *Appl. Phys. Lett.* **111**, 133111 (2017).

[22] J. Millen, T. Deesuwan, P. Barker, and J. Anders, Nanoscale temperature measurements using non-equilibrium Brownian dynamics of a levitated nanosphere, *Nature Nanotech.* **9**, 425 (2014).

[23] T. M. Hoang, J. Ahn, J. Bang, and T. Li, Electron spin control of optically levitated nanodiamonds in vacuum, *Nat. Commun.* **7**, 12250 (2016).

[24] T. Delord, L. Nicolas, M. Bodini, and G. Hétet, Diamonds levitating in a Paul trap under vacuum: Measurements of laser-induced heating via NV center thermometry, *Appl. Phys. Lett.* **111**, 013101 (2017).

[25] E. Hebestreit, R. Reimann, M. Frimmen, and L. Novotny, Measuring the internal temperature of a levitated nanoparticle in high vacuum, *Phys. Rev. A* **97**, 043803 (2018).

[26] F. Rivière, T. de Guillebon, L. Maumet, G. Hétet, M. Schmidt, J.-S. Lauret, and L. Rondin, Thermometry of an optically levitated nanodiamond, *AVS Quantum Sci.* **4**, 030801 (2022).

[27] R. Kitamura, L. Pilon, and M. Jonasz, Optical constants of silica glass from extreme ultraviolet to far infrared at near room temperature, *Appl. Opt.* **46**, 8118 (2007).

[28] J. Bateman, S. Nimmrichter, K. Hornberger, and H. Ulbricht, Near-field interferometry of a free-falling nanoparticle from a point-like source, *Nat. Commun.* **5**, 4788 (2014).

[29] H. Lee, T. Chen, J. Li, O. Painter, and K. J. Vahala, Ultra-low-loss optical delay line on a silicon chip, *Nat. Commun.* **3**, 867 (2012).

[30] J. M. Obrecht, R. J. Wild, M. Antezza, L. P. Pitaevskii, S. Stringari, and E. A. Cornell, Measurement of the temperature dependence of the Casimir–Polder force, *Phys. Rev. Lett.* **98**, 063201 (2007).

[31] C. Henkel, K. Joulain, J.-P. Mulet, and J.-J. Greffet, Radiation forces on small particles in thermal near fields, *J. Opt. A: Pure Appl. Opt.* **4**, S109 (2002).

[32] M. Antezza, L. P. Pitaevskii, and S. Stringari, New asymptotic behavior of the surface-atom force out of thermal equilibrium, *Phys. Rev. Lett.* **95**, 113202 (2005).

[33] M. Antezza, L. P. Pitaevskii, S. Stringari, and V. B. Svetovoy, Casimir–Lifshitz force out of thermal equilibrium and asymptotic nonadditivity, *Phys. Rev. Lett.* **97**, 223203 (2006).

[34] M. Antezza, L. P. Pitaevskii, S. Stringari, and V. B. Svetovoy, Casimir–Lifshitz force out of thermal equilibrium, *Phys. Rev. A* **77**, 022901 (2008).

[35] M. Krüger, T. Emig, G. Bimonte, and M. Kardar, Non-equilibrium Casimir forces: Spheres and sphere-plate, *EPL* **21002** (2011).

[36] G. Bimonte, Observing the Casimir–Lifshitz force out of thermal equilibrium, *Phys. Rev. A* **92**, 032116 (2015).

[37] G. Bimonte, T. Emig, M. Kardar, and M. Krüger, Nonequilibrium fluctuational quantum electrodynamics: Heat radiation, heat transfer, and force, *Annu. Rev. Condens. Matter Phys.* **8**, 119 (2017).

[38] C. Gonzalez-Ballester, J. Gieseler, and O. Romero-Isart, Quantum acoustomechanics with a micromagnet, *Phys. Rev. Lett.* **124**, 093602 (2020).

[39] O. Romero-Isart, A. C. Pflanzer, F. Blaser, R. Kaltenbaek, N. Kiesel, M. Aspelmeyer, and J. I. Cirac, Large quantum superpositions and interference of massive nanometer-sized objects, *Phys. Rev. Lett.* **107**, 020405 (2011).

[40] O. Romero-Isart, Quantum superposition of massive objects and collapse models, *Phys. Rev. A* **84**, 052121 (2011).

[41] Z.-q. Yin, T. Li, X. Zhang, and L. M. Duan, Large quantum superpositions of a levitated nanodiamond through spin-optomechanical coupling, *Phys. Rev. A* **88**, 033614 (2013).

[42] C. Wan, M. Scala, G. W. Morley, A. A. Rahman, H. Ulbricht, J. Bateman, P. F. Barker, S. Bose, and M. S. Kim, Free nano-object Ramsey interferometry for large quantum superpositions, *Phys. Rev. Lett.* **117**, 143003 (2016).

[43] O. Romero-Isart, Coherent inflation for large quantum superpositions of levitated microspheres, *New J. Phys.* **19**, 123029 (2017).

[44] H. Pino, J. Prat-Camps, K. Sinha, B. P. Venkatesh, and O. Romero-Isart, On-chip quantum interference of a superconducting microsphere, *Quantum Sci. Technol.* **3**, 025001 (2018).

[45] B. A. Stickler, B. Papendell, S. Kuhn, B. Schrinski, J. Millen, M. Arndt, and K. Hornberger, Probing macroscopic quantum superpositions with nanorotors, *New J. Phys.* **20**, 122001 (2018).

[46] T. Weiss, M. Roda-Llordes, E. Torrontegui, M. Aspelmeyer, and O. Romero-Isart, Large quantum delocalization of a levitated nanoparticle using optimal control: Applications for force sensing and entangling via weak forces, *Phys. Rev. Lett.* **127**, 023601 (2021).

[47] L. Neumeier, M. A. Ciampini, O. Romero-Isart, M. Aspelmeyer, and N. Kiesel, Fast quantum interference of a nanoparticle via optical potential control, *arXiv:2207.12539*.

[48] L. Hackermüller, K. Hornberger, B. Brezger, A. Zeilinger, and M. Arndt, Decoherence of matter waves by thermal emission of radiation, *Nature* **427**, 711 (2004).

[49] M. A. Schlosshauer, *Decoherence and the Quantum-to-Classical Transition*, The Frontiers Collection (Springer, Berlin ; London, 2007).

[50] A. E. Rubio López, C. Gonzalez-Ballester, and O. Romero-Isart, Internal quantum dynamics of a nanoparticle in a thermal electromagnetic field: A minimal model, *Phys. Rev. B* **98**, 155405 (2018).

[51] B. Zeng, Z. Huang, A. Singh, Y. Yao, A. K. Azad, A. D. Mohite, A. J. Taylor, D. R. Smith, and H.-T. Chen, Hybrid graphene metasurfaces for high-speed mid-infrared light modulation and single-pixel imaging, *Light Sci. Appl.* **7**, 51 (2018).

[52] Supplemental material.

[53] M. Frimmen, K. Luszcz, S. Ferreiro, V. Jain, E. Hebestreit, and L. Novotny, Controlling the net charge on a nanoparticle optically levitated in vacuum, *Phys. Rev. A* **95**, 061801 (2017).

[54] J. Vijayan, Z. Zhang, J. Piotrowski, D. Windey, F. van der Laan, M. Frimmen, and L. Novotny, Scalable all-optical cold damping of levitated nanoparticles, *arXiv:2205.04455*.

[55] S. Y. Buhmann, *Dispersion Forces. 1: Macroscopic Quantum Electrodynamics and Ground-State Casimir, Casimir–Polder and van der Waals Forces*, Springer Tracts in Modern Physics No. 247 (Springer, Berlin Heidelberg, 2012).

[56] H. B. G. Casimir and D. Polder, The influence of retardation on the London–van der Waals forces, *Phys. Rev.* **73**, 360 (1948).

[57] M. Sonnleitner, M. Ritsch-Marte, and H. Ritsch, Attractive optical forces from blackbody radiation., *Phys. Rev. Lett.* **111**, 023601 (2013).

[58] P. Haslinger, M. Jaffe, V. Xu, O. Schwartz, M. Sonnleitner, M. Ritsch-Marte, H. Ritsch, and H. Müller, Attractive force on atoms due to blackbody radiation, *Nature Phys.* **14**, 257 (2018).

[59] A. A. Geraci, S. B. Papp, and J. Kitching, Short-range force detection using optically-cooled levitated microspheres, *Phys. Rev. Lett.* **105**, 101101 (2010).

[60] V. Jain, J. Gieseler, C. Moritz, C. Dellago, R. Quidant, and L. Novotny, Direct measurement of photon recoil from a levitated nanoparticle, *Phys. Rev. Lett.* **116**, 243601 (2016).

[61] S. A. Beresnev, V. G. Chernyak, and G. A. Fomyagin, Motion of a spherical particle in a rarefied gas. Part 2. Drag and thermal polarization, *J. Fluid Mech.* **219**, 405 (1990).

[62] M. E. Gehm, K. M. O’Hara, T. A. Savard, and J. E. Thomas, Dynamics of noise-induced heating in atom traps, *Phys. Rev. A* **58**, 3914 (1998).

[63] We define the reflection coefficient $R(t, \lambda)$ as the magnitude of the Fresnel reflection coefficient at normal incidence.

[64] C. Wuttke and A. Rauschenbeutel, Thermalization via heat radiation of an individual object thinner than the thermal wavelength, *Phys. Rev. Lett.* **111**, 024301 (2013).

[65] A. O. Sushkov, W. J. Kim, D. a. R. Dalvit, and S. K. Lamoreaux, Observation of the thermal Casimir force, *Nature Phys.* **7**, 230 (2011).

[66] K. Hornberger, J. E. Sipe, and M. Arndt, Theory of decoherence in a matter wave Talbot–Lau interferometer, *Phys. Rev. A* **70**, 053608 (2004).

[67] L. Novotny and B. Hecht, *Principles of Nano-Optics* (Cambridge University Press, Cambridge, 2006).

[68] J. M. Wylie and J. E. Sipe, Quantum electrodynamics near an interface, *Phys. Rev. A* **30**, 1185 (1984).

[69] P. Virtanen, R. Gommers, T. E. Oliphant, M. Haberland, T. Reddy, D. Cournapeau, E. Burovski, P. Peterson, W. Weckesser, J. Bright, S. J. van der Walt, M. Brett, J. Wilson, K. J. Millman, N. Mayorov, A. R. J. Nelson, E. Jones, R. Kern, E. Larson, C. J. Carey, I. Polat, Y. Feng, E. W. Moore, J. VanderPlas, D. Laxalde, J. Perktold, R. Cimrman, I. Henriksen, E. A. Quintero, C. R. Harris, A. M. Archibald, A. H. Ribeiro, F. Pedregosa, and P. van Mulbregt, SciPy 1.0: Fundamental algorithms for scientific computing in Python, *Nat. Methods* **17**, 261 (2020).

[70] R. Piessens, E. de Doncker-Kapenga, C. W. Überhuber, and D. K. Kahaner, *Quadpack: A Subroutine Package for Automatic Integration* (Springer Science & Business Media, 2012).

[71] C. Gonzalez-Ballester, P. Maurer, D. Windey, L. Novotny, R. Reimann, and O. Romero-Isart, Theory for cavity cooling of levitated nanoparticles via coherent scattering: Master equation approach, *Phys. Rev. A* **100**, 013805 (2019).

[72] R. Messina, M. Tschikin, S.-A. Biehs, and P. Ben-Abdallah, Fluctuation-electrodynamical theory and dynamics of heat transfer in systems of multiple dipoles, *Phys. Rev. B* **88**, 104307 (2013).

Supplemental material

S1. DERIVATION OF THE FORCES ACTING ON THE NANOPARTICLE

In this section we give further details of the derivation of the electromagnetic forces acting on the nanoparticle that are discussed in the main text.

We consider a point dipole at position \mathbf{r}_0 with electric dipole moment given by $\mathbf{d}(t)$. The dipole is placed in vacuum and possibly in the vicinity of dielectric material (e.g. a surface). The total electromagnetic field in the space is given by $\mathbf{E}(\mathbf{r}, t)$. The electric dipole moment has a contribution $\mathbf{d}_{\text{th}}(t)$ from intrinsic thermal fluctuations at temperature T (e.g. due to the internal temperature of a nanoparticle) and a contribution $\mathbf{d}_{\text{ind}}(t)$ due to the dipole moment induced by the external electric field. The electromagnetic field $\mathbf{E}(\mathbf{r}, t)$ has a contribution $\mathbf{E}_{\text{th}}(\mathbf{r}, t)$ from environmental thermal fluctuations at temperature T_{env} (i.e. due to the temperature of the vacuum and the surrounding dielectric material), a contribution $\mathbf{E}_{\text{tw}}(\mathbf{r}, t)$ from the laser beam used for trapping, and a contribution $\mathbf{E}_{\text{ind}}(\mathbf{r}, t)$ from the field emitted by the point dipole. In total, we have

$$\mathbf{d}(t) = \mathbf{d}_{\text{th}}(t) + \mathbf{d}_{\text{ind}}(t), \quad (\text{S1})$$

$$\mathbf{E}(\mathbf{r}, t) = \mathbf{E}_{\text{th}}(\mathbf{r}, t) + \mathbf{E}_{\text{tw}}(\mathbf{r}, t) + \mathbf{E}_{\text{ind}}(\mathbf{r}, t). \quad (\text{S2})$$

In order to describe how the induced electric dipole moment depends on the electromagnetic field and vice versa, it is convenient to transform to frequency domain, defined by

$$\mathbf{d}(\omega) = \int_{-\infty}^{\infty} dt \mathbf{d}(t) e^{i\omega t}, \quad (\text{S3})$$

$$\mathbf{E}(\mathbf{r}, \omega) = \int_{-\infty}^{\infty} dt \mathbf{E}(\mathbf{r}, t) e^{i\omega t}. \quad (\text{S4})$$

The electromagnetic field emitted by the point dipole can be expressed as

$$\mathbf{E}_{\text{ind}}(\mathbf{r}, \omega) = \mathbf{G}(\mathbf{r}, \mathbf{r}_0, \omega) \mathbf{d}(\omega) = \mathbf{G}_0(\mathbf{r}, \mathbf{r}_0, \omega) \mathbf{d}(\omega) + \mathbf{G}_1(\mathbf{r}, \mathbf{r}_0, \omega) \mathbf{d}(\omega). \quad (\text{S5})$$

Here $\mathbf{G}(\mathbf{r}, \mathbf{r}_0, \omega)$ is Green's tensor for the electromagnetic field that describes the field at position \mathbf{r} emitted by the point dipole at position \mathbf{r}_0 in the presence of the surrounding material. In the second equality we used $\mathbf{G}(\mathbf{r}, \mathbf{r}_0, \omega) = \mathbf{G}_0(\mathbf{r}, \mathbf{r}_0, \omega) + \mathbf{G}_1(\mathbf{r}, \mathbf{r}_0, \omega)$, where $\mathbf{G}_0(\mathbf{r}, \mathbf{r}_0, \omega)$ is the Green's tensor in vacuum, namely in absence of any material. The Green's tensor $\mathbf{G}_1(\mathbf{r}, \mathbf{r}_0, \omega)$ is often referred to as the scattering part of the total Green's tensor.

The induced electric dipole moment can be expressed as

$$\begin{aligned} \mathbf{d}_{\text{ind}}(\omega) &= \alpha(\omega) \mathbf{E}_{\text{ex}}(\mathbf{r}_0, \omega) \\ &= \alpha(\omega) [\mathbf{E}(\mathbf{r}_0, \omega) - \mathbf{G}_0(\mathbf{r}_0, \mathbf{r}_0, \omega) \mathbf{d}(\omega)] \\ &= \alpha(\omega) [\mathbf{E}_{\text{th}}(\mathbf{r}_0, \omega) + \mathbf{E}_{\text{tw}}(\mathbf{r}_0, \omega) + \mathbf{G}_1(\mathbf{r}_0, \mathbf{r}_0, \omega) \mathbf{d}(\omega)]. \end{aligned} \quad (\text{S6})$$

Here $\alpha(\omega)$ is the scalar polarizability of the electric point dipole. The electromagnetic field inducing the dipole is given by the so called exciting field defined as $\mathbf{E}_{\text{ex}}(\mathbf{r}, \omega) \equiv \mathbf{E}(\mathbf{r}, \omega) - \mathbf{G}_0(\mathbf{r}, \mathbf{r}_0, \omega) \mathbf{d}(\omega)$. In this way, the dipole can be induced either by the external thermal field, the laser beam, or by the field emitted by the dipole that is reflected by the nearby material.

The instantaneous electromagnetic force acting on the point dipole can be evaluated as [67]

$$\mathbf{F}(t) = \sum_{j \in \{x, y, z\}} d_j(t) \nabla_{\mathbf{r}} E_{\text{ex}, j}(\mathbf{r}, t) \Big|_{\mathbf{r}=\mathbf{r}_0} + \frac{d}{dt} [\mathbf{d}(t) \cdot \mathbf{B}(\mathbf{r}_0, t)] = \nabla_{\mathbf{r}} [\mathbf{d}(t) \cdot \mathbf{E}_{\text{ex}}(\mathbf{r}, t)] \Big|_{\mathbf{r}=\mathbf{r}_0} + \frac{d}{dt} [\mathbf{d}(t) \cdot \mathbf{B}(\mathbf{r}_0, t)]. \quad (\text{S7})$$

This is a fluctuating force due to the thermal fluctuations of the dipole $\mathbf{d}_{\text{th}}(t)$ and the electric field $\mathbf{E}_{\text{th}}(\mathbf{r}, t)$. We are interested in the time-averaged value of the force $\mathbf{F} = \langle \mathbf{F}(t) \rangle$. The thermally fluctuating quantities are assumed to be both stationary and ergodic, hence the time average is equivalent to an ensemble average. Stationarity implies that the total time derivative of the second term in $\mathbf{F}(t)$ is zero under time average. Thus, one has

$$\mathbf{F} = \langle \nabla_{\mathbf{r}} [\mathbf{d}(t) \cdot \mathbf{E}_{\text{ex}}(\mathbf{r}, t)] \Big|_{\mathbf{r}=\mathbf{r}_0} \rangle = \frac{1}{4\pi^2} \int_{-\infty}^{\infty} \int_{-\infty}^{\infty} d\omega d\omega' \nabla_{\mathbf{r}} \langle \mathbf{d}(\omega) \cdot \mathbf{E}_{\text{ex}}^*(\mathbf{r}, \omega') \rangle \Big|_{\mathbf{r}=\mathbf{r}_0}, \quad (\text{S8})$$

where the quantity $\langle \mathbf{d}(\omega) \cdot \mathbf{E}_{\text{ex}}^*(\mathbf{r}, \omega') \rangle$ is the ensemble average over the realisations of the fluctuations in frequency space.

In order to evaluate the frequency correlators in the integrand of Eq. (S8), we insert Eq. (S5) and Eq. (S6) into the frequency-domain versions of Eq. (S1) and Eq. (S2) and solve for $\mathbf{d}(\omega)$ and $\mathbf{E}(\mathbf{r}, \omega)$. The result is

$$\mathbf{d}(\omega) = \mathbb{T}(\mathbf{r}_0, \omega) \{ \mathbf{d}_{\text{th}}(\omega) + \alpha(\omega)[\mathbf{E}_{\text{th}}(\mathbf{r}_0, \omega) + \mathbf{E}_{\text{tw}}(\mathbf{r}_0, \omega)] \}, \quad (\text{S9})$$

$$\mathbf{E}_{\text{ex}}(\mathbf{r}, \omega) = \mathbf{E}_{\text{th}}(\mathbf{r}, \omega) + \mathbf{E}_{\text{tw}}(\mathbf{r}, \omega) + \mathbb{G}_1(\mathbf{r}, \mathbf{r}_0, \omega) \mathbb{T}(\mathbf{r}_0, \omega) \{ \mathbf{d}_{\text{th}}(\omega) + \alpha(\omega)[\mathbf{E}_{\text{th}}(\mathbf{r}_0, \omega) + \mathbf{E}_{\text{tw}}(\mathbf{r}_0, \omega)] \}, \quad (\text{S10})$$

where

$$\mathbb{T}(\mathbf{r}_0, \omega) \equiv [\mathbb{1} - \alpha(\omega) \mathbb{G}_1(\mathbf{r}_0, \mathbf{r}_0, \omega)]^{-1}. \quad (\text{S11})$$

The tensor \mathbb{T} accounts for the ability of the dipole to scatter the radiation that it previously has emitted and that returns to the dipole after having been reflected by the environment (e.g. surface).

To understand the action of \mathbb{T} in more detail, we can introduce the “bare” dipole moment $\mathbf{d}^{(0)}$ as

$$\mathbf{d}^{(0)}(\omega) = \mathbf{d}_{\text{th}}(\omega) + \alpha(\omega)[\mathbf{E}_{\text{th}}(\mathbf{r}_0, \omega) + \mathbf{E}_{\text{tw}}(\mathbf{r}_0, \omega)]. \quad (\text{S12})$$

Next, recall that $\mathbb{G}\mathbf{d}^{(0)}$ is the field radiated by the bare dipole, and in particular, that $\mathbb{G}_1\mathbf{d}^{(0)}$ is the radiation from the bare dipole that is subsequently reflected by the environment. The dipole moment that this field induces when it returns to the dipole is $\alpha\mathbb{G}_1\mathbf{d}^{(0)}$. Therefore, we introduce the n :th induced dipole moment as

$$\mathbf{d}^{(n)}(\omega) = \alpha(\omega)\mathbb{G}_1(\mathbf{r}_0, \mathbf{r}_0, \omega)\mathbf{d}^{(n-1)}(\omega). \quad (\text{S13})$$

In words, the dipole $\mathbf{d}^{(n)}$ is the dipole moment that gets induced when radiation from the dipole $\mathbf{d}^{(n-1)}$ gets reflected by the environment and returns to the location of the point dipole. Then we see that Eq. (S9) can be formally written as

$$\mathbf{d}(\omega) = \mathbb{T}(\mathbf{r}_0, \omega)\mathbf{d}^{(0)}(\omega) = \mathbf{d}^{(0)}(\omega) + \sum_{n=1}^{\infty} \mathbf{d}^{(n)}(\omega). \quad (\text{S14})$$

In words, the total dipole moment is the bare dipole moment plus all the dipole moments that get induced in sequence as multiple reflections between the dipole and the environment happen. We then see that Eq. (S10) states that the total field has independent contributions from the thermal field, laser field, and the field radiated by the dipole including all the multiple scattering events of the dipole.

For sufficiently small polarizability, namely for $||\alpha\mathbb{G}_1|| \ll 1$, one can neglect the contributions of the induced dipole moments to the total dipole moment, i.e. the dipole’s rescattering of its own radiation can be neglected. In this case, expressions of the forces can be approximated by using $\mathbb{T} \approx \mathbb{1}$. Under this approximation, the field emitted by the bare dipole only gets reflected once – by the environment. Roughly speaking, the dipole feels the force from the radiation reflected by the environment, but it does not emit additional radiation due to the interaction. We will use this approximation later.

The frequency correlators in (S8) can now be evaluated in terms of the frequency correlators of the fluctuating and driving fields using Eq. (S9) and Eq. (S10). We assume that the cross-correlations of \mathbf{E}_{th} , \mathbf{E}_{tw} , and \mathbf{d}_{th} are zero, so that any expectation value with a combination of these quantities vanishes. Therefore, the only terms that are nonzero are those containing any of the following three correlators:

$$\langle d_{\text{th},j}(\omega) d_{\text{th},k}^*(\omega') \rangle = 2\pi\hbar\delta(\omega - \omega') \coth\left(\frac{\hbar\omega}{2k_B T}\right) \delta_{jk} \text{Im}\{\alpha(\omega)\}, \quad (\text{S15})$$

$$\langle E_{\text{th},j}(\mathbf{r}_0, \omega) E_{\text{th},k}^*(\mathbf{r}, \omega') \rangle = 2\pi\hbar\delta(\omega - \omega') \coth\left(\frac{\hbar\omega}{2k_B T_{\text{env}}}\right) \text{Im}\{G_{jk}(\mathbf{r}_0, \mathbf{r}, \omega)\}, \quad (\text{S16})$$

$$\langle E_{\text{tw},j}(\mathbf{r}_0, \omega) E_{\text{tw},k}^*(\mathbf{r}, \omega') \rangle = \delta(\omega - \omega') \lim_{\Delta\omega \rightarrow 0} \int_{\omega - \Delta\omega}^{\omega + \Delta\omega} d\omega'' E_{\text{tw},j}(\mathbf{r}_0, \omega) E_{\text{tw},k}^*(\mathbf{r}, \omega''). \quad (\text{S17})$$

The thermal correlators Eq. (S15) and Eq. (S16) are obtained using the fluctuation-dissipation theorem at the temperature of the point dipole and the electromagnetic field environment respectively. In the nonequilibrium situation $T \neq T_{\text{env}}$ (i.e. when the point dipole has a different temperature than its environment), this assumes local equilibrium. The relation Eq. (S17) holds for any field which is stationary after a time-average is performed. In the formulas that follow, we make the integral in Eq. (S17) implicit by defining:

$$\lim_{\Delta\omega \rightarrow 0} \int_{\omega - \Delta\omega}^{\omega + \Delta\omega} d\omega'' E_{\text{tw},j}(\mathbf{r}_0, \omega) E_{\text{tw},k}^*(\mathbf{r}, \omega'') \equiv E_{\text{tw},j}(\mathbf{r}_0, \omega) \bar{E}_{\text{tw},k}^*(\mathbf{r}, \omega). \quad (\text{S18})$$

Putting everything together, we identify five contributions to the mean force:

$$\mathbf{F} = \mathbf{F}_{\text{trap}} + \mathbf{F}_{\text{cs}} + \mathbf{F}_{\text{zpf}} + \mathbf{F}_{\text{env}} + \mathbf{F}_{\text{rad}}. \quad (\text{S19})$$

For each term on the right-hand side, we now give the general expression of the term, the expression within the $\mathbb{T} \rightarrow \mathbb{1}$ approximation, and a physical explanation of the term's appearance.

(1) The first term \mathbf{F}_{trap} is given by

$$\begin{aligned} \mathbf{F}_{\text{trap}} &= \int_0^\infty \frac{d\omega}{2\pi^2} \nabla_{\mathbf{r}} \left[\text{Re} \{ \alpha(\omega) \} \text{Re} \{ \bar{\mathbf{E}}_{\text{tw}}^*(\mathbf{r}, \omega) \cdot \mathbb{T}(\mathbf{r}_0, \omega) \mathbf{E}_{\text{tw}}(\mathbf{r}_0, \omega) \}_{\mathbf{r}=\mathbf{r}_0} \right. \\ &\quad \left. + \text{Im} \{ \alpha(\omega) \} \text{Im} \{ \bar{\mathbf{E}}_{\text{tw}}^*(\mathbf{r}, \omega) \cdot \mathbb{T}(\mathbf{r}_0, \omega) \mathbf{E}_{\text{tw}}(\mathbf{r}_0, \omega) \}_{\mathbf{r}=\mathbf{r}_0} \right] \\ &\approx \int_0^\infty \frac{d\omega}{2\pi^2} \left[\frac{1}{2} \text{Re} \{ \alpha(\omega) \} \nabla_{\mathbf{r}_0} [\bar{\mathbf{E}}_{\text{tw}}^*(\mathbf{r}_0, \omega) \cdot \mathbf{E}_{\text{tw}}(\mathbf{r}_0, \omega)] + \text{Im} \{ \alpha(\omega) \} \nabla_{\mathbf{r}} \text{Im} \{ \bar{\mathbf{E}}_{\text{tw}}^*(\mathbf{r}_0, \omega) \cdot \mathbf{E}_{\text{tw}}(\mathbf{r}, \omega) \}_{\mathbf{r}=\mathbf{r}_0} \right] \quad (\mathbb{T} \rightarrow \mathbb{1}). \end{aligned} \quad (\text{S20})$$

This term describes the optical gradient and scattering force exerted by the laser beam. In our proposal, this term will be used to trap the particle (e.g. optical tweezer). We remark that the field \mathbf{E}_{tw} describes the laser beam in the presence of the surrounding material but in the absence of the dipole.

(2) The second term \mathbf{F}_{cs} is given by

$$\begin{aligned} \mathbf{F}_{\text{cs}} &= \int_0^\infty \frac{d\omega}{2\pi^2} |\alpha(\omega)|^2 \nabla_{\mathbf{r}} \text{Re} \{ \bar{\mathbf{E}}_{\text{tw}}^*(\mathbf{r}_0, \omega) \cdot \mathbb{T}^\dagger(\mathbf{r}_0, \omega) \mathbf{G}_1^\dagger(\mathbf{r}, \mathbf{r}_0, \omega) \mathbb{T}(\mathbf{r}_0, \omega) \mathbf{E}_{\text{tw}}(\mathbf{r}_0, \omega) \}_{\mathbf{r}=\mathbf{r}_0} \\ &\approx \int_0^\infty \frac{d\omega}{2\pi^2} |\alpha(\omega)|^2 \nabla_{\mathbf{r}} \text{Re} \{ \bar{\mathbf{E}}_{\text{tw}}^*(\mathbf{r}_0, \omega) \cdot \mathbf{G}_1^\dagger(\mathbf{r}, \mathbf{r}_0, \omega) \mathbf{E}_{\text{tw}}(\mathbf{r}_0, \omega) \}_{\mathbf{r}=\mathbf{r}_0} \quad (\mathbb{T} \rightarrow \mathbb{1}). \end{aligned} \quad (\text{S21})$$

This force arises due to the nanoparticle scattering light from the trapping laser beam, which is subsequently reflected from the environment, and returns to interact with the nanoparticle's dipole moment. This is very similar to the force observed in [14], but here the interaction is between the nanoparticle and its optical mirror image rather than between two distinct nanoparticles. Note that the force depends on the orientation of the electric field at the position of the dipole, that is, on the polarization of the laser beam.

(3) The third term \mathbf{F}_{zpf} is given by

$$\begin{aligned} \mathbf{F}_{\text{zpf}} &= \int_0^\infty \frac{\hbar d\omega}{\pi} \nabla_{\mathbf{r}} \text{Tr} \left\{ \text{Re} \{ \alpha(\omega) \mathbb{T}(\mathbf{r}_0, \omega) \} \text{Im} \{ \mathbf{G}(\mathbf{r}_0, \mathbf{r}, \omega) \} \right. \\ &\quad \left. + \text{Re} \{ \mathbb{T}^\dagger(\mathbf{r}_0, \omega) \mathbf{G}_1(\mathbf{r}, \mathbf{r}_0, \omega) \mathbb{T}(\mathbf{r}_0, \omega) \} (\text{Im} \{ \alpha(\omega) \} + |\alpha(\omega)|^2 \text{Im} \{ \mathbf{G}(\mathbf{r}_0, \mathbf{r}_0, \omega) \}) \right\}_{\mathbf{r}=\mathbf{r}_0} \\ &\approx \int_0^\infty \frac{\hbar d\omega}{2\pi} \left\{ \text{Im} \{ \alpha(\omega) \} \nabla_{\mathbf{r}_0} \text{Tr} \{ \mathbf{G}_1(\mathbf{r}_0, \mathbf{r}_0, \omega) \} + 2|\alpha(\omega)|^2 \nabla_{\mathbf{r}} \text{Tr} [\text{Re} \{ \mathbf{G}_1(\mathbf{r}, \mathbf{r}_0, \omega) \} \text{Im} \{ \mathbf{G}(\mathbf{r}_0, \mathbf{r}_0, \omega) \}]_{\mathbf{r}=\mathbf{r}_0} \right\}. \end{aligned} \quad (\text{S22})$$

This force arises due to the quantum zero-point fluctuations of the dipole moment of the nanoparticle correlating with the zero-point fluctuations of the environmental electromagnetic field. In the $\mathbb{T} \rightarrow \mathbb{1}$ approximation, the first and second terms combine into the $\text{Im} \{ \alpha \text{Tr} \{ \mathbf{G}_1 \} \}$ term. It is typically this contribution to the force that is referred to by the name zero-temperature Casimir–Polder force [68].

(4) The fourth term \mathbf{F}_{env} contains all the dependence on the environmental temperature T_{env} and is given by

$$\begin{aligned} \mathbf{F}_{\text{env}} &= \int_0^\infty \frac{2\hbar d\omega}{\pi} n(T_{\text{env}}, \omega) \nabla_{\mathbf{r}} \text{Tr} \left\{ \text{Re} \{ \alpha(\omega) \mathbb{T}(\mathbf{r}_0, \omega) \} \text{Im} \{ \mathbf{G}(\mathbf{r}_0, \mathbf{r}, \omega) \} \right. \\ &\quad \left. + |\alpha(\omega)|^2 \text{Re} \{ \mathbb{T}^\dagger(\mathbf{r}_0, \omega) \mathbf{G}_1(\mathbf{r}, \mathbf{r}_0, \omega) \mathbb{T}(\mathbf{r}_0, \omega) \} \text{Im} \{ \mathbf{G}(\mathbf{r}_0, \mathbf{r}_0, \omega) \} \right\}_{\mathbf{r}=\mathbf{r}_0} \\ &\approx \int_0^\infty \frac{\hbar d\omega}{\pi} n(T_{\text{env}}, \omega) \left\{ \text{Re} \{ \alpha(\omega) \} \text{Im} \{ \nabla_{\mathbf{r}_0} \text{Tr} \{ \mathbf{G}(\mathbf{r}_0, \mathbf{r}_0, \omega) \} \} \right. \\ &\quad \left. + 2|\alpha(\omega)|^2 \nabla_{\mathbf{r}} \text{Tr} [\text{Re} \{ \mathbf{G}_1(\mathbf{r}, \mathbf{r}_0, \omega) \} \text{Im} \{ \mathbf{G}(\mathbf{r}_0, \mathbf{r}_0, \omega) \}]_{\mathbf{r}=\mathbf{r}_0} \right\} \quad (\mathbb{T} \rightarrow \mathbb{1}). \end{aligned} \quad (\text{S23})$$

This force arises due to environmental thermal radiation being scattered by the dipole. The first term in the force describes a gradient-type force on the total dipole due to the gradient of the thermal field intensity, and the second term is the thermal version of \mathbf{F}_{cs} , where the dipole scatters light from the thermal field which is then reflected and returns to interact with the dipole.

(5) Finally, the fifth term \mathbf{F}_{rad} contains all dependence on the particle temperature T and is given by

$$\begin{aligned}\mathbf{F}_{\text{rad}} &= \int_0^\infty \frac{2\hbar d\omega}{\pi} n(T, \omega) \text{Im}\{\alpha(\omega)\} \nabla_{\mathbf{r}} \text{Re} \left\{ \text{Tr} \left[\mathbb{T}^\dagger(\mathbf{r}_0, \omega) \mathbb{G}_1^\dagger(\mathbf{r}, \mathbf{r}_0, \omega) \mathbb{T}(\mathbf{r}_0, \omega) \right] \right\}_{\mathbf{r}=\mathbf{r}_0} \\ &\approx \int_0^\infty \frac{\hbar d\omega}{\pi} n(T, \omega) \text{Im}\{\alpha(\omega)\} \nabla_{\mathbf{r}_0} \text{Re} \left\{ \text{Tr} \left[\mathbb{G}_1^\dagger(\mathbf{r}_0, \mathbf{r}_0, \omega) \right] \right\} \quad (\mathbb{T} \rightarrow \mathbb{1}).\end{aligned}\quad (\text{S24})$$

where $n(T, \omega) = [\exp(\hbar\omega/k_B T) - 1]^{-1}$ and in the second line we used $\nabla_{\mathbf{r}} \text{Tr}[\mathbb{G}(\mathbf{r}, \mathbf{r}_0)] = \nabla_{\mathbf{r}_0} \text{Tr}[\mathbb{G}(\mathbf{r}_0, \mathbf{r}_0)]/2$. This force arises due to thermal radiation emitted by the dipole which is reflected by the environment and returns to interact with the dipole. In order for this force to be non-vanishing, the thermal radiation that returns to the dipole must retain some coherence with the dipole. This is possible for *colored* thermal emitters, meaning that $\text{Im}\{\alpha(\omega)\}$ is peaked in the infrared part of the spectrum. We emphasize that the gradient and scattering force that the dipole would experience due to its reflected field are not included in the $\mathbb{T} \rightarrow \mathbb{1}$ expression, but are part of negligible higher-order terms. To see this, it is useful to use the n :th induced thermal dipole moment and field akin to Eq. (S13): $\mathbf{d}_{\text{th}}^{(n)} = \alpha \mathbf{E}_{\text{th}}^{(n-1)}$ and $\mathbf{E}_{\text{th}}^{(n)} = \mathbb{G}_1 \mathbf{d}_{\text{th}}^{(n)}$. Then,

$$\mathbf{F}_{\text{rad}} \propto \langle \mathbf{d}_{\text{th}}^* \cdot \mathbb{G}_1 \mathbf{d}_{\text{th}} \rangle = \left\langle \left(\mathbb{T} \mathbf{d}_{\text{th}}^{(0)} \right)^* \cdot \mathbb{G}_1 \mathbb{T} \mathbf{d}_{\text{th}}^{(0)} \right\rangle = \left\langle \mathbf{d}_{\text{th}}^{(0)*} \cdot \mathbf{E}_{\text{th}}^{(0)} \right\rangle + \left\langle \mathbf{d}_{\text{th}}^{(0)*} \cdot \mathbf{E}_{\text{th}}^{(1)} \right\rangle + \alpha \left\langle \mathbf{E}_{\text{th}}^{(0)*} \cdot \mathbf{E}_{\text{th}}^{(0)} \right\rangle + \dots \quad (\text{S25})$$

where in the last expression we included terms up to first order in $\mathbf{d}_{\text{th}}^{(1)}$. The term $\mathbf{d}_{\text{th}}^{(0)*} \cdot \mathbf{E}_{\text{th}}^{(0)}$ is the coherent interaction included in the $\mathbb{T} \rightarrow \mathbb{1}$ expression, the term $\mathbf{d}_{\text{th}}^{(0)*} \cdot \mathbf{E}_{\text{th}}^{(1)}$ is the next-order coherent interaction term, while the term $\alpha \mathbf{E}_{\text{th}}^{(0)*} \cdot \mathbf{E}_{\text{th}}^{(0)}$ is the lowest-order gradient and scattering force on the nanoparticle due to the thermal emission. As we will see later, in Fig. S1, the last two terms are negligible compared to the first term.

S2. EVALUATION OF FORCES FOR A NANOPARTICLE IN A PLANE GEOMETRY

We explain how we evaluate the forces in the particular scenario of an optically trapped nanoparticle in front of a surface. The scattering Green's function above a planar interface is given by [55]

$$\mathbb{G}_1(\mathbf{r}, \mathbf{r}', \omega) = \frac{i}{8\pi^2 \epsilon_0} \int_0^\infty dk_{\parallel} \frac{k_{\parallel}}{k_z} \int_0^{2\pi} d\theta \exp\{ik_{\parallel}(\cos\theta \mathbf{e}_x + \sin\theta \mathbf{e}_y) \cdot (\mathbf{r} - \mathbf{r}') + ik_z(z + z')\} \mathbb{M}(k_{\parallel}, \theta, \omega), \quad (\text{S26})$$

with $k_z = [(\omega/c)^2 - k_{\parallel}^2]^{1/2}$ ($\text{Im}\{k_z\} > 0$), and

$$\mathbb{M}(k_{\parallel}, \theta, \omega) = \begin{pmatrix} k^2 r_s \sin^2 \theta - k_z^2 r_p \cos^2 \theta & -k^2 r_s \sin \theta \cos \theta - k_z^2 r_p \sin \theta \cos \theta & -k_p k_z r_p \cos \theta \\ -k^2 r_s \sin \theta \cos \theta - k_z^2 r_p \sin \theta \cos \theta & k^2 r_s \cos^2 \theta - k_z^2 r_p \sin^2 \theta & -k_p k_z r_p \sin \theta \\ k_p k_z r_p \cos \theta & k_p k_z r_p \sin \theta & k_p^2 r_p \end{pmatrix}, \quad (\text{S27})$$

where $r_{s,p} = r_{s,p}(k_{\parallel}, \omega)$ are the Fresnel reflection coefficients for s and p polarizations. $\mathbb{G}_1(\mathbf{r}_0, \mathbf{r}_0, \omega)$ becomes a diagonal matrix after evaluation of the θ -integral, since $\int_0^{2\pi} \mathbb{M}(k_{\parallel}, \theta, \omega) d\theta \equiv \bar{\mathbb{M}}(k_{\parallel}, \omega)$ is a diagonal matrix. Consequently, $\mathbb{T}(\mathbf{r}_0, \omega) = [1 - \alpha \mathbb{G}_1(\mathbf{r}_0, \mathbf{r}_0, \omega)]^{-1}$ is also a diagonal matrix, and the trace in Eq. (S24) can be evaluated as the trace of \mathbb{G}_1 weighted with the components of the diagonal matrices:

$$\text{Tr} \left\{ \mathbb{T}^\dagger(\mathbf{r}_0, \omega) \mathbb{G}_1(\mathbf{r}, \mathbf{r}_0, \omega)^\dagger \mathbb{T}(\mathbf{r}_0, \omega) \right\} = \sum_{j \in \{x, y, z\}} G_{1,jj}^*(\mathbf{r}, \mathbf{r}_0, \omega) |T_{jj}(\mathbf{r}_0, \omega)|^2. \quad (\text{S28})$$

Now,

$$\begin{aligned}\lim_{\mathbf{r} \rightarrow \mathbf{r}_0} \nabla_{\mathbf{r}} G_{1,jj}(\mathbf{r}, \mathbf{r}_0, \omega) &= \frac{i}{8\pi^2 \epsilon_0} \int_0^\infty dk_{\parallel} \frac{k_{\parallel}}{k_z(k_{\parallel})} e^{2ik_z(k_{\parallel})z_0} \int_0^{2\pi} d\theta \begin{pmatrix} ik_{\parallel} \cos \theta \\ ik_{\parallel} \sin \theta \\ ik_z(k_{\parallel}) \end{pmatrix} M_{jj}(k_{\parallel}, \theta, \omega) \\ &= \frac{-\mathbf{e}_z}{8\pi^2 \epsilon_0} \int_0^\infty dk_{\parallel} k_{\parallel} e^{2ik_z(k_{\parallel})z_0} \bar{M}_{jj}(k_{\parallel}, \omega),\end{aligned}\quad (\text{S29})$$

since the \mathbf{e}_x and \mathbf{e}_y components in the middle equation integrate to zero. We remark that, as the right-hand-side of Eq. (S29) is equal to $\nabla_{\mathbf{r}_0} G_{1,jj}(\mathbf{r}_0, \mathbf{r}_0)/2$, this is an explicit demonstration of the general relationship

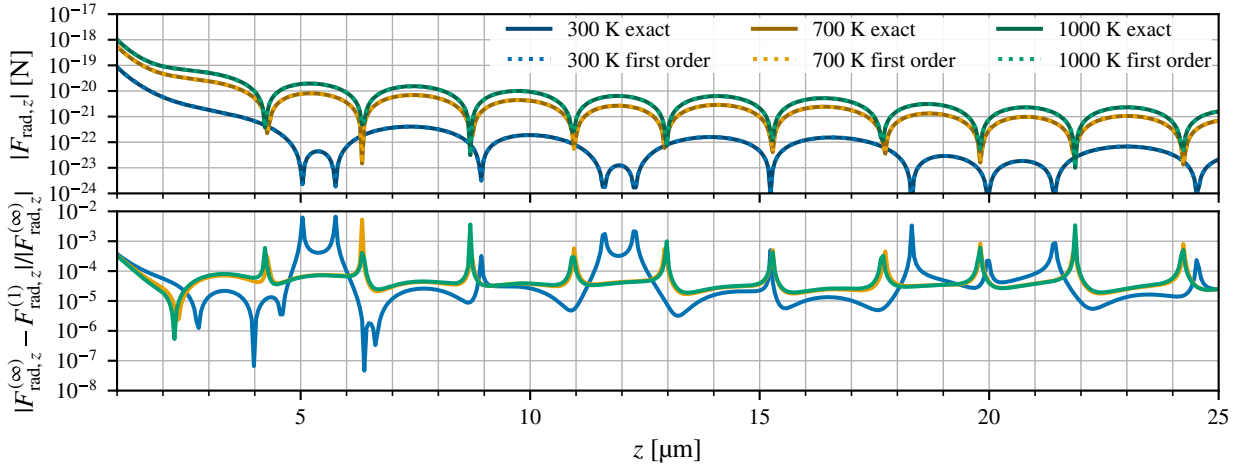


FIG. S1. Comparison of \mathbf{F}_{rad} calculated using the $\mathbb{T} \neq \mathbb{1}$ expression ($\mathbf{F}_{\text{rad}}^{(\infty)}$) and the $\mathbb{T} = \mathbb{1}$ expansion ($\mathbf{F}_{\text{rad}}^{(1)}$) of Eq. (S24). Top panel: Darker solid lines are the exact result and lighter dotted lines are the $\mathbb{T} = \mathbb{1}$ results. Bottom panel: the difference of these results as a fraction of $\mathbf{F}_{\text{rad}}^{(\infty)}$ is displayed with colors matching temperatures in the top panel.

$\lim_{\mathbf{r} \rightarrow \mathbf{r}_0} \nabla_{\mathbf{r}} G_{1,jj}(\mathbf{r}, \mathbf{r}_0, \omega) = \nabla_{\mathbf{r}_0} G_{1,jj}(\mathbf{r}_0, \mathbf{r}_0, \omega)/2$ that we used to simplify the $\mathbb{T} = 1$ expressions in Section S1. Consequently,

$$\begin{aligned} \lim_{\mathbf{r} \rightarrow \mathbf{r}_0} \nabla_{\mathbf{r}} \text{Tr} \left\{ \text{Re} \left\{ \mathbb{T}^\dagger(\mathbf{r}_0, \omega) \mathbb{G}_1(\mathbf{r}, \mathbf{r}_0, \omega)^\dagger \mathbb{T}(\mathbf{r}_0, \omega) \right\} \right\} \\ = \frac{-\mathbf{e}_z}{8\pi^2\epsilon_0} \sum_{j \in \{x,y,z\}} \text{Re} \left\{ \int_0^\infty dk_{\parallel} k_{\parallel} e^{2ik_z(k_{\parallel})z_0} \overline{M}_{jj}(k_{\parallel}, \omega) \right\} |T_{jj}(\mathbf{r}_0, \omega)|^2, \end{aligned} \quad (\text{S30})$$

with

$$\overline{M}_{xx}(k_{\parallel}, \omega) = \overline{M}_{yy}(k_{\parallel}, \omega) = \pi((\omega/c)^2 r_s(k_{\parallel}, \omega) - k_z^2(k_{\parallel}) r_p(k_{\parallel}, \omega)), \quad \overline{M}_{zz}(k_{\parallel}, \omega) = 2\pi k_{\parallel}^2 r_p(k_{\parallel}, \omega), \quad (\text{S31})$$

$$(T_{jj})^{-1} = 1 - \frac{i\alpha(\omega)}{8\pi^2\epsilon_0} \int_0^\infty dk_{\parallel} \frac{k_{\parallel}}{k_z(k_{\parallel})} e^{2ik_z(k_{\parallel})z_0} \overline{M}_{jj}(k_{\parallel}, \omega). \quad (\text{S32})$$

Insertion of Eqs. (S30-S32) into Eq. (S24) would now allow numerical evaluation of the integrals. However, we proceed to the special case of a perfectly reflecting plane which has $r_s(k_{\parallel}, \omega) = -1$, $r_p(k_{\parallel}, \omega) = 1$. In this case the integrals over k_{\parallel} can be performed analytically, and we obtain, with $k = \omega/c$

$$\lim_{\mathbf{r} \rightarrow \mathbf{r}_0} \nabla_{\mathbf{r}} G_{1,jj}(\mathbf{r}, \mathbf{r}_0, \omega) = -\frac{\mathbf{e}_z e^{2ikz_0}}{64\pi\epsilon_0 z_0^4} \begin{cases} 3 - 6ikz_0 - 8k^2 z_0^2 + 8ik^3 z_0^3 & j = x, y \\ 6 - 12ikz_0 - 8k^2 z_0^2 & j = z \end{cases} \quad (\text{S33})$$

$$(T_{jj}(\mathbf{r}_0, \omega))^{-1} = \begin{cases} 1 + \alpha(\omega) e^{2ikz_0} (-1 + 2ikz_0 + 4k^2 z_0^2) / (32\pi\epsilon_0 z_0^3) & j = x, y \\ 1 + i\alpha(\omega) e^{2ikz_0} (i + 2kz_0) / (16\pi\epsilon_0 z_0^3) & j = z \end{cases} \quad (\text{S34})$$

Usage of these relations with Eq. (S30) leaves only the ω integral to be evaluated in Eq. (S24). We use these relations to investigate the accuracy of the $\mathbb{T} = 1$ version of (S24) to the expression including \mathbb{T} . The $\mathbb{T} = 1$ expansions of Eqs. (S21-S22) are conveniently evaluated for a perfectly reflecting plane by using

$$\nabla_{\mathbf{r}_0} \text{Tr} \left\{ \mathbb{G}_1(\mathbf{r}_0, \mathbf{r}_0, \omega) \right\} = \frac{\mathbf{e}_z}{8\pi\epsilon_0 z_0^4} e^{2ikz_0} (-3 + 6ikz_0 + 6k^2 z_0^2 - 4ik^3 z_0^3) \quad (\text{S35})$$

which can be obtained from Eq. (S33) combined with $\lim_{\mathbf{r} \rightarrow \mathbf{r}_0} \nabla_{\mathbf{r}} G_{1,jj}(\mathbf{r}, \mathbf{r}_0, \omega) = \nabla_{\mathbf{r}_0} G_{1,jj}(\mathbf{r}_0, \mathbf{r}_0, \omega)/2$, or from the method of images. We compare the $\mathbb{T} \neq \mathbb{1}$ and $\mathbb{T} = \mathbb{1}$ results for \mathbf{F}_{rad} in Figure S1. We find agreement between the full and expanded results, as expected for a subwavelength particle since it fulfills $|\alpha \mathbb{G}_1| \ll 1$. Therefore we use the $\mathbb{T} = \mathbb{1}$ versions of all forces in the rest of this work.

We evaluate the total force on the nanoparticle \mathbf{F} displayed in Figure 2 in the main text as follows: Starting from (S19), we neglect \mathbf{F}_{trap} since its later effect on the PSD is captured by the trapping frequency Ω and equilibrium

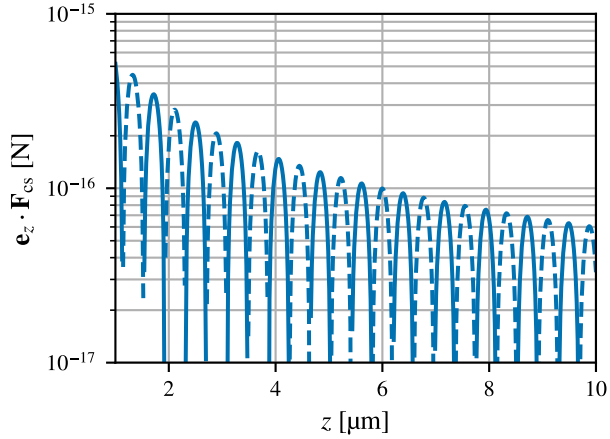


FIG. S2. \mathbf{F}_{cs} for a nanoparticle above a surface which reflects the tweezer wavelength λ_0 perfectly. Solid/dashed lines indicate that the force is positive/negative in the normal direction of the surface.

position \mathbf{r}_0 . \mathbf{F}_{rad} and \mathbf{F}_{env} were calculated using (S24) and (S23) with (S35) and $\alpha(\omega)$ as displayed in Fig. 1(c) in the main text. In (S23), we neglect the term $\propto |\alpha(\omega)|^2$. We performed the integrals numerically using the Gauss–Kronrod 21-point rule as implemented in the `scipy.integrate.quad_vec` method of SciPy 1.8.0 [69, 70]. As integration bounds we used the upper and lower bounds $\lambda_{\text{max}} = 50 \mu\text{m}$ and $\lambda_{\text{min}} = 7 \mu\text{m}$ of the $\epsilon(\lambda)$ dataset [27], translated into frequency space as $\omega_{\text{min,max}} = 2\pi c/\lambda_{\text{max,min}}$. We evaluate \mathbf{F}_{zpf} with the far-field approximation of the Casimir force

$$\mathbf{F}_{\text{zpf}}(z \gg r) = -\frac{\hbar c \alpha(0)}{8\pi^2 z^5} \mathbf{e}_z \quad (\text{S36})$$

where r is the nanoparticle radius and with $\alpha(0)$ derived from the electrostatic value $\epsilon(0) = 3.8$ of the permittivity of SiO_2 . The well-known formula Eq. (S36) can be derived analytically from Eq. (S22) (neglecting the integrand term $\propto |\alpha(\omega)|^2$) by performing a Wick rotation of the integral in (S22) onto the imaginary axis to obtain a non-oscillating, rapidly decaying integrand and then expanding the result for $z > \lambda$ where λ is the minimum wavelength appearing in the integral [56, 68]. As a consistency check, we compared a full numerical evaluation of the Wick-rotated (S22) (translating $\alpha(\omega)$ to the imaginary axis using the Schwarz formula $\alpha(i\omega) = \frac{2}{\pi} \int_0^\infty \phi \text{Im}\{\alpha(\phi)\} / (\phi^2 + \omega^2) d\phi$, $\omega \in \mathbb{R}$) to the approximation Eq. (S36) and found excellent agreement, confirming that the Casimir force is dominated by the electrostatic value of the polarizability also in the present case.

To evaluate \mathbf{F}_{cs} , we approximate the optical tweezer by the time-harmonic function $\mathbf{E}_{\text{tw}}(\mathbf{r}, t) = E_{\text{tw}}(\mathbf{r}) \mathbf{e}_x \cos(\omega_0 t)$, where we assume the tweezer beam to be polarized parallel to the plane, consistent with the geometry of our proposed setup. This enables us to remove the integral in (S21) to find

$$\mathbf{F}_{\text{cs}} = \frac{|\alpha(\omega_0)|^2}{2} |E_{\text{tw}}(\mathbf{r}_0)|^2 \text{Re} \left\{ \lim_{\mathbf{r} \rightarrow \mathbf{r}_0} \nabla_{\mathbf{r}} G_{1,xx}(\mathbf{r}, \mathbf{r}_0, \omega_0) \right\}. \quad (\text{S37})$$

The field intensity at the center of the tweezer is given in terms of the experimental parameters as $|E_{\text{tw}}(\mathbf{r}_0)|^2 = 2\pi N^2 P_{\text{tw}} / \epsilon_0 c \lambda_0^2$. We calculate the \mathbf{F}_{cs} that would result if the surface was perfectly reflecting at $\lambda_0 = 2\pi c/\omega_0$. The force would then become

$$\mathbf{F}_{\text{cs}} = -\mathbf{e}_z \left| \frac{\alpha(\lambda_0)}{\epsilon_0} \right|^2 \frac{N^2 P_{\text{tw}}}{64 c \lambda_0^2 z_0^4} j_x(2\pi z_0 / \lambda_0) \quad (\text{S38})$$

with $j_x(x) = \text{Re} \{ \exp(2ix)(3 - 6ix - 8x^2 + 8ix^3) \}$. We plot this force in Figure S2. However, in our scenario the surface is transparent at ω_0 and the optical interaction force will be weaker. We approximate the magnitude of the optical interaction force above our non-perfectly reflecting surface as $|r_{\perp}(\omega_0) \mathbf{F}_{\text{cs}}|$, where $r_{\perp}(\omega_0)$ is the reflection coefficient of the surface at ω_0 and normal incidence, and the symbol \mathbf{F}_{cs} retains its meaning as the coherent scattering force above a perfectly reflecting plane.

We model the modulation of the surface reflectivity in time as follows. We assume that the presence of the surface gives rise to a Green's tensor which is effectively the Green's tensor above a perfectly reflecting surface in the range

$(\omega_{\text{peak}} - \Gamma, \omega_{\text{peak}} + \Gamma)$ (where $\omega_{\text{peak}} = 2\pi c/\lambda_{\text{peak}}$ is the frequency of the dominant peak of $n(\omega, T) \text{Im}\{\alpha(\omega)\}$ in the temperatures of interest and Γ is the full width at half maximum (FWHM) of the peak), but where the Fresnel coefficients obtain a sinusoidal oscillation about their perfect reflector values with amplitude η and frequency Ω_d : for $\omega \in (\omega_{\text{peak}} - \Gamma, \omega_{\text{peak}} + \Gamma)$,

$$\begin{cases} r_s(\omega, k_{\parallel}) = -1 \rightarrow -(1 - \frac{\eta}{2}[1 - \cos(\Omega_d t)]), \\ r_p(\omega, k_{\parallel}) = 1 \rightarrow 1 - \frac{\eta}{2}[1 - \cos(\Omega_d t)]. \end{cases} \quad (\text{S39})$$

Since the integral giving \mathbf{F}_{rad} is dominated by the value of the integrand in this range, this effectively gives

$$\mathbf{F}_{\text{rad}} \rightarrow (1 - \frac{\eta}{2})\mathbf{F}_{\text{rad}} + \frac{\eta}{2} \cos(\Omega_d t)\mathbf{F}_{\text{rad}} \quad (\text{S40})$$

in the expression (S19). Note that the symbol \mathbf{F}_{rad} retains its meaning as the strength of the force above a perfectly reflecting surface. \mathbf{F}_{env} also obtains a time-dependence in this way, but we neglect investigating it since $|\mathbf{F}_{\text{rad}}| \gg |\mathbf{F}_{\text{env}}|$ when $T > T_{\text{env}}$. We assume that \mathbf{F}_{zpf} does not obtain a time-dependence, since we have seen that it is sensitive only to the electrostatic limit of the integrand. Ideally, \mathbf{F}_{cs} would not obtain a time-dependence since the surface would be perfectly transparent at ω_0 at all times. However, the modulation of the reflection coefficients at ω_{peak} will realistically also lead to a residual modulation of the reflection coefficients at ω_0 , which in turn would give rise to a time-dependent force $|r_{\perp}(t, \omega_0)\mathbf{F}_{\text{cs}}|$ due to the interaction with the nanoparticle's optical image. As we will see later in Section S4, to measure \mathbf{F}_{rad} we require it to dominate the Ω_d frequency component of the total time-dependent force on the nanoparticle. We make this condition quantitative by defining the amplitude of the Ω_d frequency component of the driving of $|r_{\perp}(\omega_0)|$ as $\eta_0 \equiv \lim_{T \rightarrow \infty} T^{-1} \int_{-T}^T dt \cos(\Omega_d t)|r_{\perp}(t, \omega_0)|$. This gives the condition $|\mathbf{F}_{\text{cs}}|\eta_0 \ll |\mathbf{F}_{\text{rad}}|\eta$ where roughly $|\mathbf{F}_{\text{rad}}|/|\mathbf{F}_{\text{cs}}| \sim 10^{-4}$. If the driving of the reflection coefficients at thermal frequencies is not perfectly sinusoidal, one should consider the η appearing in this condition to be defined in an equivalent manner to η_0 . Assuming the condition on η and η_0 to hold, the relevant effect of the time-dependent reflection coefficients on the total force \mathbf{F} is

$$\mathbf{F} \rightarrow \mathbf{F} - \frac{\eta}{2}\mathbf{F}_{\text{rad}} + \frac{\eta}{2} \cos(\Omega_d t)\mathbf{F}_{\text{rad}}. \quad (\text{S41})$$

To simplify the presentation in the main text, we defined the reflection coefficient $R(t, \lambda)$ to be the magnitude of the Fresnel reflection coefficient at normal incidence: $R(t, \lambda) = |r_s(2\pi c/\lambda, 0; t)| = |r_p(2\pi c/\lambda, 0; t)| = |r_{\perp}(2\pi c/\lambda, 0; t)|$. We remark that the reflectivity of the surface at normal incidence is given by $R^2(t, \lambda)$.

S3. NANOPARTICLE POLARIZABILITY AND ITS LORENTZIAN APPROXIMATION

We obtain $\alpha(\lambda)$ from measurements of the relative permittivity $\epsilon(\lambda)$ of fused silica glass in the bulk summarized in [27]. $\alpha(\lambda)$ is calculated from these data via the quasistatic polarizability for a dielectric sphere

$$\alpha(\lambda) = 3\epsilon_0 V \frac{\epsilon(\lambda) - 1}{\epsilon(\lambda) + 2}. \quad (\text{S42})$$

The model in [27] gives values of $\text{Im}\{\epsilon(\lambda)\}$ in the optical range $\lambda \in [1, 7] \mu\text{m}$ which are lower than the measurements reported in the optical range in the same work. However, we have checked that the values of $\epsilon(\lambda)$ in the optical range are so small that including them in our model for $\alpha(\lambda)$ does not affect the results for the forces. Rather, we observe that the integrands giving the values of the forces are dominated by $\alpha(\lambda)$ at its peak values; the value of \mathbf{F}_{rad} is especially dominated by the peak of $\epsilon(\lambda)$ around $\lambda_{\text{peak}} = 8.9 \mu\text{m}$. To confirm this, we fit a frequency-domain Lorentzian model

$$\alpha_L(\omega) = 3\epsilon_0 V \frac{\omega_p^2}{\omega_{\text{peak}}^2 - \omega^2 - i\Gamma\omega}, \quad (\text{S43})$$

to this peak in the frequency-domain version of Eq. (S42). Here $\omega_{\text{peak}}, \omega_p$ and Γ are all real parameters. Specifically, we fit $\text{Im}\{\alpha_L(\omega)\}$ to $\text{Im}\{\alpha(\omega)\}$ using the `scipy.optimize.curve_fit` method of SciPy 1.8.0 [69], obtaining the peak frequency $\omega_0 = 2\pi \times 3.4 \times 10^{13} \text{ Hz}$, the linewidth $\Gamma = 2\pi \times 1.5 \times 10^{12} \text{ Hz}$ and $\omega_p = 2\pi \times 8.8 \times 10^{12} \text{ Hz}$. Γ corresponds to a linewidth $2\pi c\Gamma/\omega_{\text{peak}}^2 = 0.4 \mu\text{m}$ of $\alpha_L(\lambda)$. We then use α_L to compute \mathbf{F}_{rad} approximately and compare to the results using α , finding good agreement, which confirms that the peak at ω_{peak} dominates the integral for \mathbf{F}_{rad} .

Using α_L , we also investigate the effect on \mathbf{F}_{rad} of broadening the linewidth of the peak, which gives insight into the role of colored emission on the strength of \mathbf{F}_{rad} . In Fig. S3(a) we plot $\text{Im}\{\alpha_L(\lambda; n)\}$ where $\alpha_L(\lambda; n)$ is given by

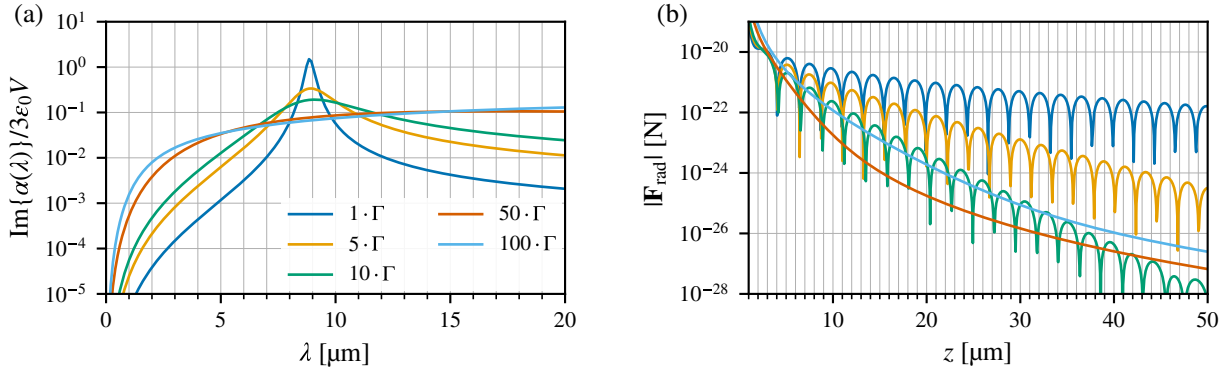


FIG. S3. The effect of broadening the linewidth of the Lorentzian fit on \mathbf{F}_{rad} . (a) The broadened lorentzians. The factor in the legend indicates the linewidth with respect to the original linewidth Γ . The broadened Lorentzians are renormalized in order to keep the total power radiated by the nanoparticle constant. (b) \mathbf{F}_{rad} calculated using the Lorentzian of the corresponding color in panel (a) and $T = 600$ K.

Eq. (S43) with $\Gamma \rightarrow n\Gamma$ and renormalized to keep the total radiated power constant (see Eq. (S69)), and in Fig. S3(b) the \mathbf{F}_{rad} calculated using these polarizabilities. We find that as the linewidth is increased, the scaling of the force decreases progressively to z^{-6} , i.e. a weaker scaling than the z^{-5} far-field Casimir force, and the oscillations in sign vanish.

S4. SENSING OF \mathbf{F}_{rad}

For low temperatures of the center of mass motion, an optically trapped nanoparticle is well-modelled as a damped harmonic oscillator. The equation of motion of a driven damped harmonic oscillator with position $x(t)$ is

$$\ddot{x} + \gamma\dot{x} + \Omega^2 x = \frac{1}{m} [F(t) + K(t)]. \quad (\text{S44})$$

where γ is the total damping rate of the nanoparticle's motion, $F(t)$ is a deterministic driving force and $K(t)$ is the sum of all the noise forces. By Fourier transform, we can solve this equation to be

$$x(\omega) = \chi(\omega) [F(\omega) + K(\omega)], \quad (\text{S45})$$

$$\chi(\omega) = \frac{1}{m(\Omega^2 - \omega^2 - i\gamma\omega)}. \quad (\text{S46})$$

Introducing the motional and force PSDs

$$S_{xx}(\omega) = \frac{1}{2\pi} \int_{-\infty}^{\infty} \langle x(t)x(t+\tau) \rangle e^{i\omega\tau} d\tau, \quad (\text{S47})$$

$$S_F(\omega) = \frac{1}{2\pi} \int_{-\infty}^{\infty} \langle F(t)F(t+\tau) \rangle e^{i\omega\tau} d\tau, \quad (\text{S48})$$

$$S_K(\omega) = \frac{1}{2\pi} \int_{-\infty}^{\infty} \langle K(t)K(t+\tau) \rangle e^{i\omega\tau} d\tau, \quad (\text{S49})$$

one can show that the motional PSD can be expressed in terms of the force PSDs as

$$S_{xx}(\omega) = |\chi(\omega)|^2 [S_F(\omega) + S_K(\omega)]. \quad (\text{S50})$$

From this, we can define the thermally limited signal-to-noise ratio (SNR) as

$$\text{SNR} = \frac{S_F(\omega)}{S_K(\omega)}. \quad (\text{S51})$$

The square root of $S_F(\omega)$ at $\text{SNR} = 1$ is called the force sensitivity \mathcal{S} and is given by

$$\mathcal{S}(\omega) = \sqrt{S_K(\omega)}, \quad (\text{S52})$$

and has units of $\text{N}/\sqrt{\text{Hz}}$.

To find the force PSD, we assume a harmonic driving force

$$F(t) = A(z, T) \cos(\Omega_d t + \phi), \quad (\text{S53})$$

with Ω_d the driving frequency and ϕ the initial phase of the driving, and where we find from Eq. (S41) the amplitude $A(z, T)$ to be

$$A(z, t) = \frac{\eta}{2} [\mathbf{e}_z \cdot \mathbf{F}_{\text{rad}}(z, T)]. \quad (\text{S54})$$

From this, one calculates the force PSD

$$S_F(\omega) = \frac{A^2(z, T)}{4} [\delta(\omega + \Omega_d) + \delta(\omega - \Omega_d)]. \quad (\text{S55})$$

A perfectly harmonic driving force is an idealization that does not exist in experiments. Any realistic approximately harmonic driving force will have some drift or error in its driving frequency Ω_d , which smoothens the δ -functions appearing in (S55). We can account for the uncertainty in Ω_d by broadening the δ -functions in (S55) into Lorentzians with linewidth Γ_d which represent the broadening:

$$\delta(\omega \pm \Omega_d) \rightarrow \frac{1}{\pi} \frac{\Gamma_d}{(\omega \pm \Omega_d)^2 + \Gamma_d^2}. \quad (\text{S56})$$

We can check the validity of this broadening by taking the $\Gamma_d \rightarrow 0$ limit of the RHS using the Plemejl formula, and seeing that it recovers the LHS. This results in the PSD

$$S_F(\omega) = \frac{A^2(z, T)}{4\pi} \left[\frac{\Gamma_d}{(\omega + \Omega_d)^2 + \Gamma_d^2} + \frac{\Gamma_d}{(\omega - \Omega_d)^2 + \Gamma_d^2} \right]. \quad (\text{S57})$$

The contributions to the noise force $K(t)$ that we model are random collisions with the gas and photon shot noise [60, 71]. Thus,

$$S_K(\omega) = S_{\text{photon}}(\omega) + S_{\text{gas}}(\omega), \quad (\text{S58})$$

$$S_{\text{photon}}(\omega) = \frac{2}{5} \frac{\hbar\omega_0}{2\pi c^2} P_{\text{scatt}}, \quad (\text{S59})$$

$$S_{\text{gas}}(\omega) = \frac{m\gamma_{\text{gas}}k_{\text{B}}T_{\text{gas}}}{\pi}. \quad (\text{S60})$$

Here ω_0 is the frequency of the trapping laser, P_{scatt} is the power scattered from the tweezer laser, γ_{gas} is the damping rate due to gas collisions, and T_{gas} is the temperature of the gas. The power scattered from the tweezer laser is given by $P_{\text{scatt}} = \sigma_{\text{scatt}} I_0$, where σ_{scatt} is the electromagnetic scattering cross-section of the nanoparticle, and I_0 is the intensity at the trapping laser focus. These two quantities are given by [60]

$$I_0 = \frac{P_{\text{tw}}\omega_0^2 N^2}{2\pi c^2}, \quad (\text{S61})$$

$$\sigma_{\text{scatt}} = \frac{\omega_0^4 |\alpha(\omega_0)|^2}{6\pi c^4 \epsilon_0^2}. \quad (\text{S62})$$

Here N is the numerical aperture of the trap. The gas damping rate is given by [61]

$$\gamma_{\text{gas}} = 0.619 \frac{6\pi r^2}{m} p \sqrt{\frac{2m_{\text{gas}}}{\pi k_{\text{B}} T_{\text{gas}}}}. \quad (\text{S63})$$

Here r is the nanoparticle radius, p is the gas pressure, m_{gas} is the gas molecular mass. Inserting our expressions for the noise PSDs into the expression for \mathcal{S} , we obtain

$$\mathcal{S} = \sqrt{\frac{\hbar\omega_0^7 |\alpha(\omega_0)|^2 N^2 P_{\text{tw}}}{60\pi^3 \epsilon_0^2 c^8} + 6 \cdot 0.619 r^2 p \sqrt{\frac{2m_{\text{gas}} k_{\text{B}} T_{\text{gas}}}{\pi}}}. \quad (\text{S64})$$

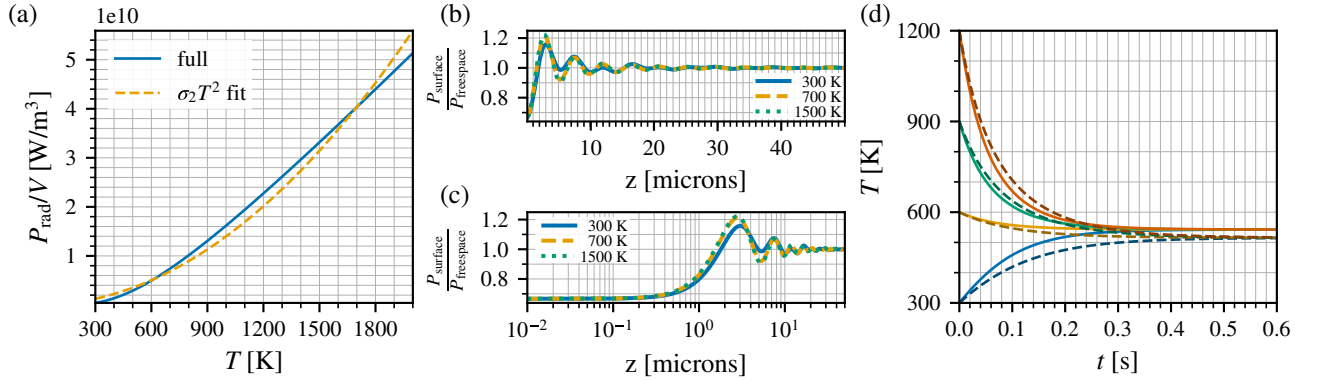


FIG. S4. (a) The power radiated per volume by an SiO_2 nanoparticle in free space in the temperature range relevant for experiments, as well as a quadratic fit from 300 to 2000 K which we use to qualitatively understand the nanoparticle thermodynamics. (b) The power emitted above a perfectly reflecting surface as a fraction of the power emitted in free space. (c) The same function as in panel (b), but with a log-scaled horizontal axis. (d) Time evolution of the temperature in the radiative cooling regime for the parameters in the main text. Colors denote different initial temperatures. Solid lines are numerical solutions of Eq. (S66), dashed lines are the approximation Eq. (S71). The numerical steady state temperature is 543 K while the approximation gives $T_\infty = 515$ K.

Putting everything together, we arrive at the expression for the signal-to-noise ratio evaluated at the driving frequency Ω_d

$$\begin{aligned} \text{SNR}(\Omega_d) &= \frac{A^2(z, T)}{4\pi\Gamma_d} \left(\frac{\hbar\omega_0^7 |\alpha(\omega_0)|^2 N^2 P_{\text{tw}}}{60\pi^3 \epsilon_0^2 c^8} + 6 \cdot 0.619 r^2 p \sqrt{\frac{2m_{\text{gas}}\pi k_B T_{\text{gas}}}{\pi}} \right)^{-1} \\ &\approx \frac{\eta^2 [\mathbf{e}_z \cdot \mathbf{F}_{\text{rad}}(z, T)]^2}{16\pi\Gamma_d} \left(\frac{\hbar\omega_0^5 |\alpha(\omega_0)|^2 I_0}{30\pi^2 \epsilon_0^2 c^6} \right)^{-1} \end{aligned} \quad (\text{S65})$$

where in the second row we assumed that we are below the pressure at which \mathcal{S} becomes photon shot noise-dominated. This expression lets us identify the scaling of the SNR with the experimental parameters. In this analysis, we assume a constant T independently controllable from the other parameters. Since $|\mathbf{F}_{\text{rad}}| \propto |\alpha| \propto V$, the SNR is independent of the particle size. Increasing the laser intensity I_0 at the nanoparticle decreases the SNR since the photon shot noise increases.

S5. HEAT BALANCE EQUATION FOR THE NANOPARTICLE

Our goal in this section is to capture the behavior of the temperature dynamics predicted by fluctuational electrodynamics in a simple, qualitative model. We predict the temperature dynamics of the nanoparticle for our experimental parameters using the heat balance equation

$$c_m \rho V \frac{dT}{dt} = P_{\text{abs}} - P_{\text{rad}}(T), \quad (\text{S66})$$

where we use $c_m = 700 \text{ J/kg}$ for SiO_2 , and

$$P_{\text{abs}} = P_{\text{abs,tw}} + P_{\text{abs,env}}(T_{\text{env}}), \quad (\text{S67})$$

Here $P_{\text{abs,env}}(T_{\text{env}})$ is the power that the nanoparticle absorbs from environmental radiation, and $P_{\text{abs,tw}}$ is the power that the nanoparticle absorbs from the laser beam. The latter is

$$P_{\text{abs,tw}} = \frac{\omega_0 \text{Im} \{ \alpha(\omega_0) \}}{c} I_0. \quad (\text{S68})$$

As can be calculated using $P_{\text{rad}}(T) - P_{\text{abs,env}}(T_{\text{env}}) = \langle [\partial_t \mathbf{d}(t)] \cdot \mathbf{E}(t) \rangle$ (see e.g. [72]), in free space

$$P_{\text{rad}}(T) = \frac{\hbar c^2}{\pi^2} \int_0^\infty dk \frac{k^4}{e^{\hbar ck/k_B T} - 1} \text{Im} \{ \alpha(ck) \}, \quad (\text{S69})$$

and $P_{\text{abs,env}}(T_{\text{env}}) = P_{\text{rad}}(T_{\text{env}})$. We have not included the correction to Eq. (S69) from radiation reaction (see [50] and references therein) because it gives negligible corrections for the material and particle size that we consider. With our parameters, $P_{\text{abs,env}}(T_{\text{env}}) \ll P_{\text{abs,tw}}$, so we neglect $P_{\text{abs,env}}(T_{\text{env}})$. We obtain a simplified model of $P_{\text{rad}}(T)$ for the silica nanoparticle by approximating it as a quadratic function of T :

$$P_{\text{rad}}(T) \approx \sigma_2 V T^2, \quad (\text{S70})$$

where we find $\sigma_2 = 2 \times 10^4 \text{ W/m}^3 \text{K}^2$ by numerical fit to (S69). We display Eq. (S69) and compare it to the quadratic approximation Eq. (S70) in Fig. S4(a). $P_{\text{rad}}(T)$ is in general affected by the presence of dielectric material like the surface. As an example, we plot $P_{\text{rad}}(T)$ for our silica nanoparticle above a perfectly reflecting surface in Fig. S4(b) and (c). The emitted power oscillates with z with a maximum change of 20% for $z > 1 \mu\text{m}$. The qualitative behavior of the temperature dynamics will not be affected by this change, so we find that Eq. (S70) still qualitatively captures the emitted power for this example. To make a qualitative model of the temperature dynamics, we insert Eq. (S70) into (S66). This gives a simple instance of Riccati's equation for T with solution

$$T(t) = \begin{cases} T_\infty \tanh [t/\tau + \text{artanh}(T_0/T_\infty)] & (T_\infty > T_0) \\ T_\infty \coth [t/\tau + \text{artanh}(T_\infty/T_0)] & (T_\infty < T_0) \end{cases} \quad (\text{S71})$$

where the time constant is

$$\tau = \frac{\rho c_m}{\sqrt{\frac{P_{\text{abs}}}{V} \sigma_2}}, \quad (\text{S72})$$

and $T_\infty = \sqrt{P_{\text{abs}}/V\sigma_2}$. Note that P_{abs}/V is independent of V . In Fig. S4(d) we compare time trajectories of the temperature obtained with numerical solution of Eq. (S66) and with the approximation Eq. (S71). We find that the approximation reproduces the qualitative behavior of the trajectories and that the final temperature agrees within 30 K.